

# Adiabatic fission barriers in superheavy nuclei

P. Jachimowicz

*Institute of Physics, University of Zielona Góra, Szafrana 4a, 65516 Zielona Góra, Poland*

M. Kowal\* and J. Skalski

*National Centre for Nuclear Research, Hoża 69, PL-00-681 Warsaw, Poland*

(Dated: June 16, 2016)

Using the microscopic-macroscopic model based on the deformed Woods-Saxon single-particle potential and the Yukawa-plus-exponential macroscopic energy we calculated static fission barriers  $B_f$  for 1305 heavy and superheavy nuclei  $98 \leq Z \leq 126$ , including even - even, odd - even, even - odd and odd - odd systems. For odd and odd-odd nuclei, adiabatic potential energy surfaces were calculated by a minimization over configurations with one blocked neutron or/and proton on a level from the 10-th below to the 10-th above the Fermi level. The parameters of the model that have been fixed previously by a fit to masses of even-even heavy nuclei were kept unchanged. A search for saddle points has been performed by the "Imaginary Water Flow" method on a basic five-dimensional deformation grid, including triaxiality. Two auxiliary grids were used for checking the effects of the mass asymmetry and hexadecapole non-axiality. The ground states were found by energy minimization over configurations and deformations. We find that the non-axiality significantly changes first and second fission barrier in many nuclei. The effect of the mass - asymmetry, known to lower the second, very deformed barriers in actinides, in the heaviest nuclei appears at the less deformed saddles in more than 100 nuclei. It happens for those saddles in which the triaxiality does not play any role, what suggests a decoupling between effects of the mass-asymmetry and triaxiality. We studied also the influence of the pairing interaction strength on the staggering of  $B_f$  for odd- and even-particle numbers. Finally, we provide a comparison of our results with other theoretical fission barrier evaluations and with available experimental estimates.

PACS numbers: 25.70.Jj, 25.70.Gh, 25.85.Ca, 27.90.+b

## I. INTRODUCTION

Although fission barrier heights  $B_f$  are not directly measurable quantities, i.e. are not quantum observables, they are very useful in estimating nuclear fission rates. As the activation energy  $E_a$  (per mole) in chemistry gives a rate  $k$  of a chemical reaction at temperature  $T$  via the Arrhenius law:  $k = Ae^{-E_a/RT}$  ( $R$  - the gas constant;  $A$  - the frequency factor) [1, 2], the fission barrier gives the fission rate  $\Gamma_f$  of an excited (as they usually are in nuclear reactions) nucleus via:  $\Gamma_f \sim e^{-B_f/kT_{eff}}$ , where  $T_{eff}$  is an effective temperature derived from the excitation energy, and  $k$  - the Boltzman constant. For example, knowing fission barriers of possible fusion products helps predicting a cross section for a production of a given evaporation residue in a heavy ion reaction: one can figure out whether neutron or alpha emission wins a competition with fission at each stage of the deexcitation of a compound nucleus. Moreover, one can try to understand the experimentally established, intriguing growth of the total cross sections around  $Z=118$ ; for its correlation with  $B_f$ , see e.g. Fig. 6 and the related discussion in [3]. On the other hand, the prediction of the spontaneous or low energy (i.e. from a weakly excited state) fission rates, governed by the regime of the collective quantum tunneling, requires an additional knowledge of the barrier

shape and mass parameters.

A non-observable status of the fission barrier, again in analogy to that of the activation energy in chemistry, is reflected in its possible dependence on a reaction type and/or the excitation energy (effective temperature) range. This leads to some uncertainty in calculations of fission barriers. In particular, it is not clear whether intrinsic configurations should be conserved along the level crossings, which increases  $B_f$ , or the adiabatic state should be followed. This is especially relevant for odd- $A$  and odd-odd nuclei, in which sharp crossings of levels occupied by the odd particle exclude the strictly adiabatic scenario. It is known that if the projection of the single-particle angular momentum on the symmetry axis of a nucleus  $\Omega$  is conserved, the diabatic effect on the fission barrier can be huge, see e.g. [4]. As there is no accepted formula for a barrier correction due to the non-adiabaticity, it is usually ignored, even in odd- $N$  and/or odd- $Z$  nuclei. A general idea is that at the excitation energies close to, and higher than the barrier, but still not inducing sizable dissipative corrections, the adiabatic barrier could be used for calculating fission rates.

Since calculations of potential energy surfaces (PES's) for odd- $A$  and odd-odd nuclei involve a repetition of calculations for many low-lying quasiparticle states which multiplies the effort (especially in odd-odd systems), systematic studies of their fission barriers are rather scarce. Up to now, they were provided mainly by the Los Alamos microscopic-macroscopic (MM) model and recently by some self-consistent models [5]. The current state of the-

---

\*Electronic address: m.kowal@fuw.edu.pl

oretical predictions in fission of even - even nuclei (with  $Z \geq 100$ ) has been discussed recently in [6].

In the present paper we extend our MM model based on the deformed Woods-Saxon potential, which up to now was applied mainly to even-even nuclei [7], to odd- $A$  and odd-odd SH systems. We study a wide range of isotopes which, perhaps, may be of some use for astrophysical purposes. The fission barriers are calculated using the adiabatic assumption, i.e. they are the smallest possible. Since the model has been quite reasonable, in particular in reproducing first [7] and second [8] fission barriers in actinides, as well as super- [9] and hyper-deformed [10, 11] minima, we prefer to keep its parameters unchanged. The shell and pairing correction for an odd nucleon system is done by blocking the lowest-lying quasiparticle states. The modification of the macroscopic energy by including the average pairing energy contribution which we introduced for nuclear masses in [12] is irrelevant for fission barriers.

The other motivation of our study is to improve the predictions for the fission saddles. This requires simultaneously taking into account a large number of shape variables [8, 11] and relying on an *in principle* exact method for finding saddles to escape errors inherent in the mostly used constrained minimization method, see [13, 14]. As usual, to make the involved computational effort manageable one has to make some compromises which will be discussed in detail. The need for a simultaneous consideration of many shape variables in PES's calculations is common to all nuclear models, including self-consistent theories based on some effective interactions [15]. The results on fission saddles obtained up to now in the SH region clearly show the great importance of triaxial deformation, neglected in many published work. A recent study [16] of barriers within both the MM Woods-Saxon and Skyrme SLy6 Hartree-Fock plus BCS models shows that triaxiality is even more crucial beyond  $Z = 126$ .

A description of our method of calculations is given in section II. The results, details of the additional calculations, and comparisons with other calculated barriers are presented and discussed in section III. Finally, the conclusions are summarized in section IV.

## II. THE METHOD

Multidimensional energy landscapes are calculated within the MM model based on the deformed Woods-Saxon potential [17]. The Strutinski shell and pairing correction [18] is taken for the microscopic part. For the macroscopic part we used the Yukawa plus exponential model [19] with parameters specified in [20]. Thus, all parameter values are kept exactly the same as in all recent applications of the model to heavy and superheavy nuclei

The main point in fission barrier calculations is its reliability which, once the model for calculating energy of a nucleus as a function of deformation is fixed, hangs on

two main ingredients: 1) the kind and dimension of the admitted deformation space and 2) a method applied to the search for saddles.

Mononuclear shapes can be parameterized via spherical harmonics  $Y_{lm}(\vartheta, \varphi)$  (for brevity we will just use the symbol  $Y_{\lambda\mu}$ ) by the following equation of the nuclear surface:

$$R(\vartheta, \varphi) = c(\{\beta\})R_0\{1 + \sum_{\lambda=1}^{\infty} \sum_{\mu=-\lambda}^{+\lambda} \beta_{\lambda\mu} Y_{\lambda\mu}\}, \quad (1)$$

where  $c(\{\beta\})$  is the volume-fixing factor and  $R_0$  is the radius of a spherical nucleus. This parameterization has its limitations; certainly, it is not suitable for too elongated shapes. However, for moderately deformed saddle points in superheavy nuclei it excellently reproduces all shapes generated by other parametrizations, e.g. by [21], as we checked in numerous tests.

For nuclear ground states it is possible to confine analysis to axially-symmetric shapes, with the expansion truncated at  $\beta_{80}$ :

$$R(\vartheta, \varphi) = c(\{\beta\})R_0\{1 + \beta_{20}Y_{20} + \beta_{30}Y_{30} + \beta_{40}Y_{40} + \beta_{50}Y_{50} + \beta_{60}Y_{60} + \beta_{70}Y_{70} + \beta_{80}Y_{80}\}. \quad (2)$$

Thus, a seven dimensional minimization is performed using the gradient method. For odd systems, the additional minimization over configurations is performed at every step of the gradient procedure. Considered configurations consist of the odd particle occupying one of the levels close to the Fermi level and the rest of the particles forming a paired BCS state on the remaining levels. Ten states above and ten states below the Fermi level have been blocked and energy minimized over these configurations.

The main problem in a search for saddle points is that, since they are neither minima nor maxima, one has to know energy on a multidimensional grid of deformations (the often used and much simpler method of minimization with imposed constraints may produce invalid results [8, 13–15]). To find saddles on a grid we used the Imaginary Water Flow (IWF) technique. This conceptually simple and at the same time very efficient (from a numerical point of view) method was widely used and discussed before [8, 13, 22–25]. The number of numerically tractable deformation parameters  $\{\beta_{\lambda\mu}\}$  is practically limited. More than five-dimensional grids, keeping in mind a subsequent interpolation, are intractable in calculations for many ( $\sim 1000$ ) nuclei. Including mass- and axially-symmetric deformations ( $\beta_{20}, \beta_{40}, \beta_{60}, \beta_{80}$  - see [26–29] together with both, mass-asymmetry ( $\beta_{30}, \beta_{50}, \beta_{70}$ ) and triaxiality (at least  $\beta_{22}$ ) would mean at least an eight-dimensional mesh and was impossible at present.

Based on our previous results showing that triaxial saddles are abundant in SH nuclei [7], we consider that quadrupole triaxial shapes have to be necessarily included. We treated the effects of mass-asymmetry and

nonaxial higher multipoles as corrections and analysed them at the second stage of calculations. A rationale for a lesser importance of mass-asymmetric saddles is that, while they constitute a second, more deformed ( $\beta_{20} \approx 0.7 - 0.8$ ), prominent barrier peak in actinides, their heights are much reduced in SH nuclei where they become irrelevant. In the remaining, less deformed saddles the mass asymmetry occurs less frequently. As to the nonaxial multipoles of higher order, they are less important for saddles with small to moderate  $\gamma$  [where  $\gamma$  is the Bohr's quadrupole nonaxiality parameter, cf. Eq. (7)]. They become important for  $\gamma$  closer to  $60^\circ$  where they are needed to produce oblate shapes having  $x$  as the symmetry axis. Thus, they should be included for nuclei with a large oblate g.s. deformation and a short triaxial barrier. The additional studies of the mass-asymmetry and higher nonaxial multipoles are described in the proper subsections of the Results section.

Thus, at the first stage, for all 1305 investigated nuclei the saddle points were searched in a five dimensional deformation space spanned by:  $\beta_{20}, \beta_{22}, \beta_{40}, \beta_{60}, \beta_{80}$ , using the IWF technique. The appropriate nuclear radius expansion has the form:

$$R(\vartheta, \varphi) = c(\{\beta\})R_0\left\{1 + \beta_{20}Y_{20} + \frac{\beta_{22}}{\sqrt{2}}[Y_{22} + Y_{2-2}] + \beta_{40}Y_{40} + \beta_{60}Y_{60} + \beta_{80}Y_{80}\right\}. \quad (3)$$

The five-dimensional calculations are performed on the following deformation mesh:

$$\begin{aligned} \beta_{20} &= 0.00 \text{ (0.05) } 0.60 \\ \beta_{22} &= 0.00 \text{ (0.05) } 0.45 \\ \beta_{40} &= -0.20 \text{ (0.02) } 0.20 \\ \beta_{60} &= -0.10 \text{ (0.02) } 0.10 \\ \beta_{80} &= -0.10 \text{ (0.02) } 0.10 \end{aligned} \quad (4)$$

This makes a grid of 29250 points which was subsequently interpolated to a fivefold denser grid of 50735286 points with the step 0.01 in each dimension. On the latter, the saddle point, or rather several saddle points - if there were a few of comparable heights within the 0.5 MeV energy window - were searched for by means of the IWF procedure. For odd or odd-odd nuclei, at each grid point we were looking for low-lying configurations by blocking particles on levels from the 10-th below to the 10-th above the Fermi level (in neutrons or/and protons).

The fact that searches for ground states and for saddles are separated - performed using different deformation spaces - allows saving some number of deformation parameters in Eq. (3). This is equivalent to assuming that the fission saddles have mostly prolate deformations large enough to make nonaxial deformations of multipolarity  $\lambda \geq 3$  less important. One has to check this assumption afterwards and separately treat nuclei in which the inclusion of nonaxial deformations with  $\lambda \geq 4$  is necessary.

Although, as mentioned before, in SH nuclei the second barriers at large deformations are usually smaller than the first one or do not exist at all, for  $Z = 98-101$  the mesh (4) was extended to  $\beta_{20} = 1.5$  and the second saddles were searched for by the IWF technique. It turned out that these more deformed barriers are indeed mostly smaller than the first ones and decrease with increasing  $Z$ . Only in Cf isotopes with  $N = 134-160$  there were some second saddles (at  $\beta_{20} \approx 0.9$ ) higher than the first one by at most 0.5 MeV. However, even those saddles were lowered by at least 1 MeV after including the mass-asymmetry. Therefore, we have reasons to believe that the range of  $\beta_{20}$  in (4) is sufficient for knowing the height of the fission barrier in the whole studied region.

### III. RESULTS AND DISCUSSION

In the present paper we have systematically calculated fission-barrier heights  $B_f$  as the energy difference between the saddle point and the ground state. The saddle point is defined as the minimum over possible fission paths of the maximal energy along the path. Let us emphasize that the calculations presented here have been performed without adding any zero-point vibration energy. We have included 1305 heavy and superheavy nuclei with proton numbers  $98 \leq Z \leq 126$  and neutron numbers in the range  $134 \leq N \leq 192$ , with the smallest  $N$  for a given  $Z$  increasing by one with every step in  $Z$ . All obtained barriers have been collected in Table III. On all PES's presented here, energy is normalized in such a way that its macroscopic part is set to zero at the spherical shape.

#### A. Potential Energy surfaces

Some idea about the positions of ground states, secondary minima and saddles may be gained from PES's. Chosen examples are shown in figures for:  $^{252}\text{Lr}$  - Fig. 1,  $^{270}\text{Db}$  - Fig. 2,  $^{276}\text{Mt}$  - Fig. 3,  $^{280}\text{Cn}$  - Fig. 4, and  $^{297}119$  - Fig. 5. Overall evolution of ground states with increasing  $Z$  from prolate to spherical can be seen there. In some nuclei one can see multiple saddles of which the one defining the fission barrier should be properly chosen. Sometimes the saddles between competing minima can be important, therefore the determination of all saddles on the map is necessarily needed.

The energy landscapes Fig. 1-5 were obtained by minimizing energy on the 5D grid (3) with respect to  $\beta_{40}$ ,  $\beta_{60}$  and  $\beta_{80}$ . One should be aware of two related circumstances: 1) As the grid Eq. (3) does not include nonaxial deformations  $\lambda \geq 4$ , the axial deformations  $\lambda = 4, 6, 8$  with respect to the  $x$ -axis cannot be reproduced, so the landscapes are inexact around the oblate  $\gamma = 60^\circ$  axis. 2) A reduction of a  $n$ -dimensional grid of energy values via the minimization over  $n - 2$  deformations sometimes leads to an energy surface composed from disconnected

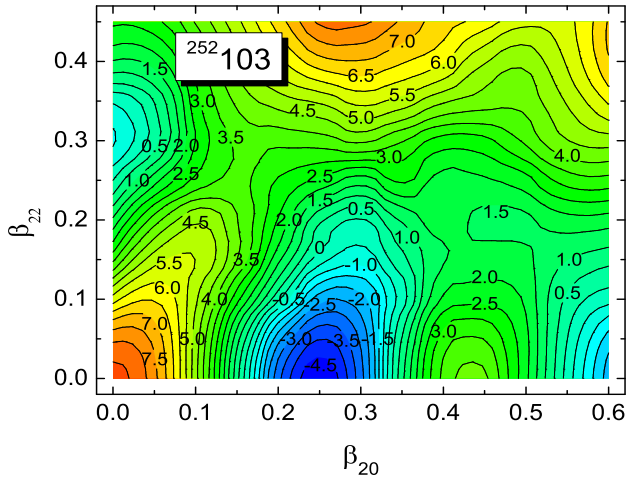


FIG. 1: Energy surface,  $E - E_{\text{mac}}(\text{sphere})$ , for  $Z = 103$  and  $N = 149$ .

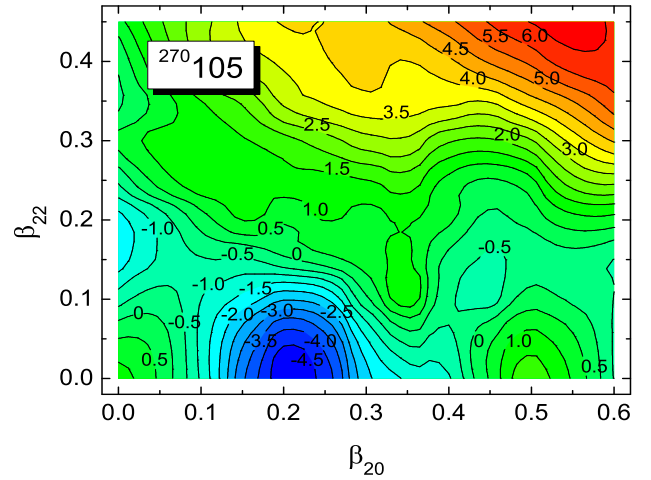


FIG. 2: The same as in 1 but for  $Z = 105$  and  $N = 165$ .

patches, corresponding to multiple minima in the auxiliary (those minimized over) dimensions. This can distort the picture of the barrier (actually, a reduction of multi-dimensional data to a two-dimensional map is a general problem).

With these reservations in mind, one can still explore some of the details shown in the maps. In particular, the prolate g.s. minimum with strongly nonaxial first saddle point at  $\beta_{20} = 0.41$  and  $\beta_{22} = 0.18$  is visible in  $^{252}\text{Lr}$ . One can notice that the axially symmetric saddle lies more than 2 MeV higher. A slightly less steep, prolate g.s. minimum and a gently emerging second minimum is visible in Fig 2 for  $^{270}\text{Db}$ . The triaxial saddle at  $\beta_{20} = 0.52$  and  $\beta_{22} = 0.13$  has a smaller triaxiality  $\gamma$  than the saddle in  $^{252}\text{Lr}$ . A decrease in barrier height due to triaxiality is  $\approx 2$  MeV, Fig. 2.

In a heavier nucleus  $^{276}\text{Mt}$ , a prolate deformation of the g.s. is clearly smaller than in  $^{252}\text{Lr}$ , see Fig 3. The second minimum, which was barely outlined in  $^{270}\text{Db}$ , is more pronounced here, giving the fission barrier a double-hump structure. The deformation  $\beta_{20} \approx 0.5$  of the second saddle is much smaller than that of the second barriers in actinides. Thus, a two-peak structure of the barrier in SH nuclei may be viewed as a result of a division (split) of the first barrier, occurring with growing  $Z$ . The higher second axial saddle is lowered by triaxiality by  $\approx 1.5$  MeV, but eventually is still higher than the first axial saddle.

For  $^{280}\text{Ds}$  a topology of the PES is even more complicated. We see several minima: prolate - the g.s. and a superdeformed one, and a shallow oblate. The map shows also a few saddles. The axially deformed saddle

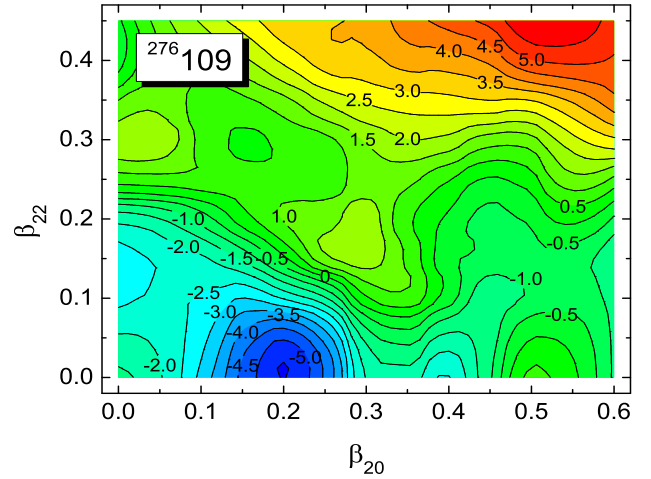


FIG. 3: The same as in 1 but for  $Z = 109$  and  $N = 167$ .

point at  $\beta_{20} = 0.3$  has a similar height as the nonaxial saddle at  $\beta_{20} = 0.54$  and  $\beta_{22} = 0.12$ . It follows from the IWF calculation that the second fission barrier is nonaxial in this case. The axial second saddle is lowered by  $\approx 1$  MeV owing to the nonaxiality.

The nucleus  $Z = 119$ ,  $N = 178$  is spherical in its g.s. - Fig. 5. There is a secondary oblate minimum (whose depth is underestimated in the map due to omission of nonaxial  $\lambda = 4, 6$  deformations). There is a low triaxial

## B. Role of the mass asymmetry

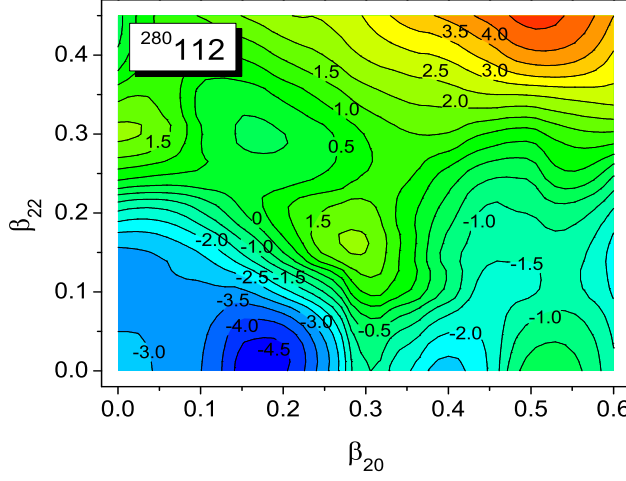


FIG. 4: The same as in 1 but for  $Z = 112$  and  $N = 168$ .

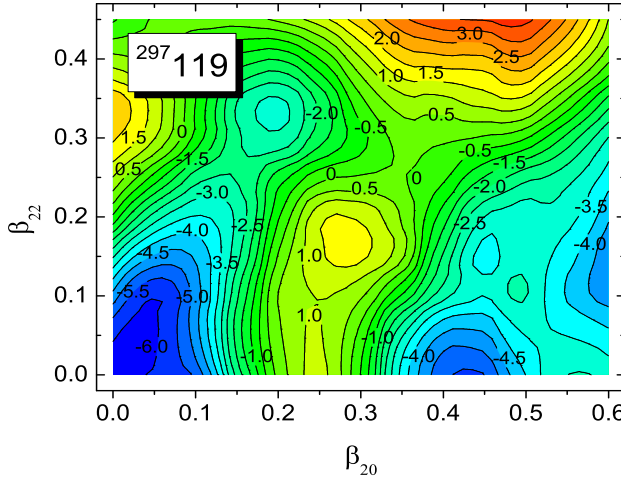


FIG. 5: The same as in 1 but for  $Z = 119$  and  $N = 178$ .

second saddle at  $\beta_{20} \approx 0.5$  and two "first saddles" with different triaxiality, of which the one with a larger  $\gamma$  is the fission saddle.

Still another type of PES, typical of nuclei with the superdeformed oblate g.s., is presented in Fig.8 in the subsection C.

To study the effect of the reflection (mass) - asymmetry on the fission barriers, a two-step procedure has been performed. At the first stage, we have checked the stability of all the saddles found on the basic 5D mesh (the first, the second, ..., axially symmetric or triaxial, of energy within 0.5 MeV of the highest saddle) against the mass-asymmetry. This was done by a 3D energy minimization with respect to  $\beta_{30}$ ,  $\beta_{50}$  and  $\beta_{70}$  around each saddle. Since most of the saddles are non-axial, the most general version of our Woods-Saxon code had to be used. In this case, when both symmetries (axial and mass symmetry) are broken simultaneously, the nuclear shapes are defined by the following equation of the nuclear surface:

$$R(\vartheta, \varphi) = R_0 c(\{\beta\}) \left\{ 1 + \beta_{20} Y_{20} + \frac{\beta_{22}}{\sqrt{2}} [Y_{22} + Y_{2-2}] \right. \\ \left. + \beta_{30} Y_{30} + \beta_{40} Y_{40} + \beta_{50} Y_{50} \right. \\ \left. + \beta_{60} Y_{60} + \beta_{70} Y_{70} + \beta_{80} Y_{80} \right\}$$

It turned out that this minimization lowers energy of only those saddles in which: i) there is no triaxiality, ii) deformation  $\beta_{20} \approx 0.3$ . This supports an often expressed conventional "wisdom", that the mass-asymmetry and triaxiality effects on fission saddle are decoupled. This is why, at the second step of the procedure, we could carry out a full IWF analysis on a grid including only axially-symmetric deformations:  $\beta_{20}, \beta_{30}, \beta_{40}, \beta_{50}, \beta_{60}, \beta_{70}, \beta_{80}$ , with  $\beta_{20}$  restricted to a quite short interval 0.25 – 0.40:

$$\begin{aligned} \beta_{20} &= 0.25 (0.05) 0.40 \\ \beta_{30} &= 0.00 (0.05) 0.25 \\ \beta_{40} &= -0.15 (0.05) 0.20 \\ \beta_{50} &= 0.00 (0.05) 0.15 \\ \beta_{60} &= -0.10 (0.05) 0.10 \\ \beta_{70} &= 0.00 (0.05) 0.15 \\ \beta_{80} &= -0.10 (0.05) 0.10. \end{aligned}$$

(6)

This seven-dimensional grid, composed of 76800 deformations, was subject to the fivefold interpolation in all directions before it was used in the IWF procedure. This means that the IWF calculations have been performed on the grid containing 1 690 730 496(!) points. We have made such 7-dimensional analysis for more than 100 nuclei, for which the effect of minimization was greater than 300 keV. Results for these nuclei are shown in Table I. The rest of 127 cases shown in Table I are the test nuclei, in which the effect of the minimization was smaller than 0.3 MeV. The results for these additional nuclei allow to appreciate whether the (in principle exact) IWF method could produce a greater effect than the (inexact) minimization.

As one can see, the adopted procedure allowed to omit the problem of searching for a saddle by using the (inexact) minimization method which is not always reliable

[8, 13]. For example, for  $Z=118$  and  $N=165$ , the discussed effect resulting from the minimization amounts to 0.44 MeV, which, just in this case, is quite similar to 0.46 MeV obtained from the IWF technique; however, in  $Z=113$  and  $N=163$  one obtains  $\approx 0.5$  MeV difference between saddles obtained by both methods. In this particular nucleus, the  $\approx 0.77$  MeV barrier lowering by the mass-asymmetry is the largest among all studied nuclei. It should be also noted that for the isotopes of  $Z = 113$  the effect of the mass-asymmetry is particularly large, see the top panel in Fig. 6.

In the bottom panel of Fig. 6, we show the difference between the results of the both methods - the minimization - (MIN) and "Imaginary Water Flow" - (IWF). One can see that this difference increases with the neutron number. In particular, there is practically no effect derived from the mass-asymmetry in  $^{281}113$  when IWF is used. On the contrary, the approach based on minimization suggests still a quite substantial (spurious) effect (0.55 MeV). One might notice that our conclusion concerning decoupling of the variables describing the axial and reflection asymmetries is in a delicate contradiction with the studies [30].

### C. Role of the triaxiality

The importance of including triaxiality in a calculation of fission barrier heights was indicated many times before [31–40]. In particular, it was shown that the effect of *both* quadrupole and a general hexadecapole nonaxiality, when accounted for within the *nonexact* method of constrained minimization (used generally in all selfconsistent studies), may reach 2.5 MeV for some superheavy even-even nuclei, see Fig. 5 in [7]. Here, we extend our previous discussion of its role to the odd and odd-odd nuclei and, at the same time, improve the treatment by employing the exact IWF method in potentially most interesting cases.

By using the original 5D mesh (4) we have obtained saddles with *quadrupole* nonaxiality for about 900 nuclei, what constitutes more than 70 % of all fission barriers. We illustrate this conspicuous effect in Fig. 7 on the example of two isotopic chains,  $Z=103$  and 113.

We show the difference between axial and nonaxial barriers in these nuclei. One can see that for lighter Lawrencium isotopes the effect of nonaxiality is quite considerable. Starting with  $N = 164$ , it is weakening quickly and finally vanishes for  $N \geq 176$ . Somewhat different dependence of the effect on the neutron number occurs in  $Z = 113$  isotopes. The maximum lowering of the barrier of more than 1.5 MeV occurs for  $N \approx 165$ , there is a second maximum at  $N = 179$ , and the effect becomes large again at  $N = 192$ . Inbetween, for  $N \approx 154$  and  $N \approx 174$ , there is no effect at all. Thus, the effect of nonaxiality has to be studied carefully, indeed.

Another task is to consider the influence of the hexadecapole nonaxiality, namely:  $\beta_{42}, \beta_{44}$  in Eq. 1, on

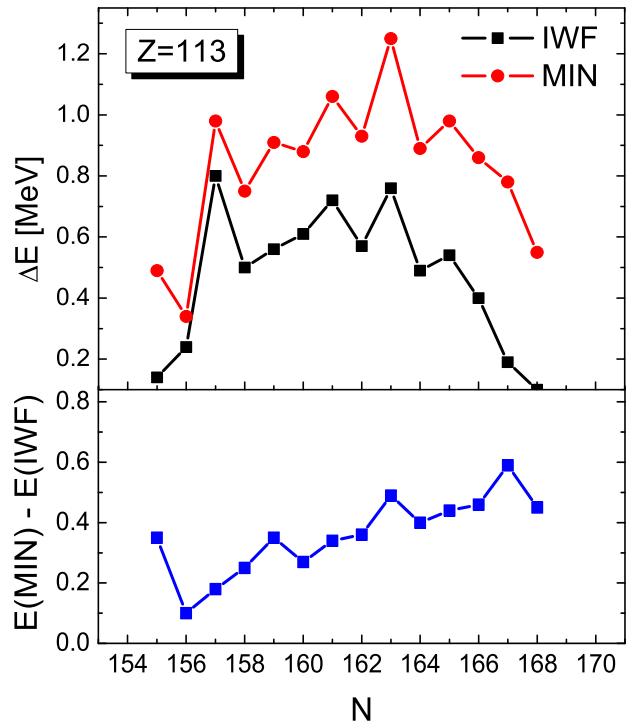


FIG. 6: Top panel: The fission barrier lowering by the mass-asymmetry obtained by the (in principle exact) Imaginary Water Flow method - IWF and by the (easier, but sometimes misleading) minimization method - MIN. Bottom panel: The difference between both methods in MeV (in principle - the error in the barrier height due to the minimization method).

the fission barriers. The unconstrained inclusion of these shapes would lead to a 7D grid which is too much for now. To evaluate the effect without increasing the grid dimension we constrained  $\beta_{42}$  and  $\beta_{44}$  to be functions of the quadrupole nonaxial deformation  $\beta_{22}$ , or actually  $\gamma$ , and  $\beta_{40}$ , in a well known manner [45]. Using the conventional notation:

$$\begin{aligned} \beta &= \sqrt{\beta_{20}^2 + \beta_{22}^2}, \\ \gamma &= \arctg \frac{\beta_{22}}{\beta_{20}}, \end{aligned} \quad (7)$$

the following form of Eq. 1 was used:

TABLE I: Mass(reflection)-asymmetry effect on the fission barrier from the minimization - MIN and from the Imaginary Water Flow method - IWF (in MeV).

N	IWF	MIN	N	IWF	MIN	N	IWF	MIN
<b>Z = 109</b>			<b>Z = 114</b>			<b>Z = 117</b>		
157	0.39	0.81	155	0.28	0.59	157	0.24	0.34
158	0.22	0.42	156	0.14	<0.30	158	0.28	<0.30
159	0.54	0.45	157	0.72	0.83	159	0.24	0.34
160	0.31	0.54	158	0.46	0.46	160	0.12	<0.30
<b>Z = 110</b>			159	0.67	0.68	161	0.26	<0.30
157	0.41	0.69	160	0.45	0.66	165	0.36	0.39
158	0.19	0.31	161	0.53	0.79	166	0.23	<0.30
159	0.52	0.46	162	0.42	0.64	167	0.19	0.50
160	0.50	0.40	163	0.58	0.65	168	0.07	<0.30
161	0.43	0.47	164	0.40	0.63	169	0.05	0.37
162	0.35	0.31	165	0.42	0.65	<b>Z = 118</b>		
<b>Z = 111</b>			166	0.38	0.53	163	0.30	0.32
157	0.49	0.97	167	0.11	0.68	164	0.23	<0.30
158	0.36	0.78	168	0.06	0.41	165	0.46	0.44
159	0.61	0.83	<b>Z = 115</b>			166	0.28	0.31
160	0.67	0.85	157	0.28	0.64	167	0.20	0.63
161	0.87	0.89	158	0.25	0.50	168	0.15	0.39
162	0.66	0.80	159	0.34	0.49	<b>Z = 119</b>		
163	0.56	0.83	160	0.39	0.38	165	0.46	0.57
164	0.58	0.68	161	0.56	0.58	166	0.33	0.37
166	0.48	0.49	162	0.42	0.39	167	0.34	0.49
<b>Z = 112</b>			163	0.46	0.54	168	0.27	0.32
157	0.57	0.83	164	0.49	0.45	169	0.31	0.57
158	0.32	0.45	165	0.47	0.60	170	0.24	0.38
159	0.58	0.55	166	0.53	0.54	171	0.23	0.32
160	0.60	0.49	167	0.42	0.80	<b>Z = 120</b>		
161	0.51	0.60	168	0.20	0.55	165	0.39	0.38
162	0.53	0.48	169	0.13	0.31	166	0.17	<0.30
163	0.56	0.64	170	0.07	0.30	167	0.20	0.49
164	0.44	0.43	<b>Z = 116</b>			168	0.15	<0.30
165	0.33	0.48	155	0.40	0.41	169	0.10	0.46
166	0.34	0.34	156	0.19	<0.30	<b>Z = 121</b>		
167	0.20	0.35	157	0.36	0.52	165	0.25	0.40
<b>Z = 113</b>			158	0.26	0.34	166	0.23	<0.30
155	0.14	0.49	159	0.35	0.44	167	0.38	0.52
156	0.24	0.34	160	0.28	0.49	168	0.31	0.34
157	0.80	0.98	161	0.40	0.44	169	0.36	0.60
158	0.50	0.75	162	0.33	0.37	170	0.30	0.43
159	0.56	0.91	163	0.48	0.54	<b>Z = 122</b>		
160	0.61	0.88	164	0.40	0.38	164	0.00	<0.30
161	0.72	1.06	165	0.46	0.50	165	0.21	<0.30
162	0.57	0.93	166	0.33	0.40	166	0.12	<0.30
163	0.76	1.25	167	0.30	0.38	167	0.19	0.31
164	0.49	0.89	168	0.11	<0.30	168	0.11	<0.30
165	0.54	0.98	169	0.09	0.32	169	0.10	0.45
166	0.40	0.86	<b>Z = 123</b>			<b>Z = 123</b>		
167	0.19	0.78				166	0.06	<0.30
168	0.10	0.55				167	0.08	0.35
			<b>Z = 124</b>			<b>Z = 124</b>		
						165	0.23	0.31
						166	0.06	<0.30
						167	0.10	0.32



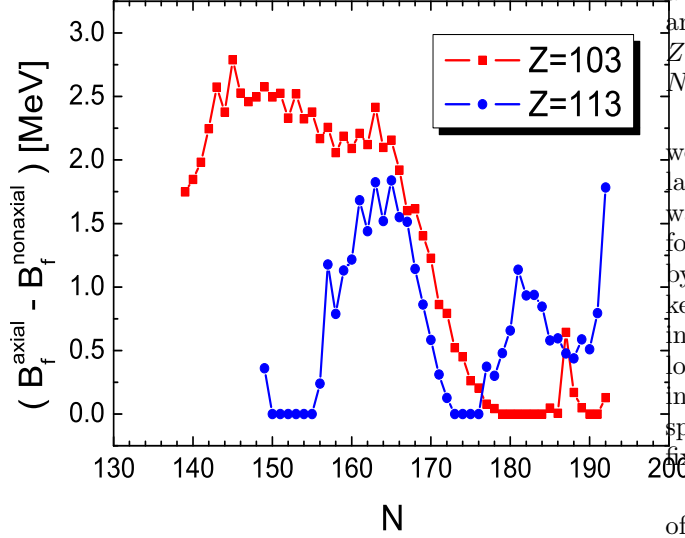


FIG. 7: Effect of the non-axiality on the fission barrier heights (see text for further explanations).

$$\begin{aligned}
 R(\vartheta, \varphi) = c(\beta)R_0 \{ & 1 + \beta \cos(\gamma)Y_{20} \\
 & + \frac{\beta \sin(\gamma)}{\sqrt{2}} [Y_{22} + Y_{2-2}] \\
 & + \beta_{40} \frac{1}{6} (5 \cos^2(\gamma) + 1) Y_{40} \\
 & - \beta_{40} \frac{1}{6} \sqrt{\frac{15}{2}} \sin(2\gamma) [Y_{42} + Y_{4-2}] \\
 & + \beta_{40} \frac{1}{6} \sqrt{\frac{35}{2}} \sin^2(\gamma) [Y_{44} + Y_{4-4}] \\
 & + \beta_{60} Y_{60} + \beta_{80} Y_{80} \}. \quad (8)
 \end{aligned}$$

On this 5D grid, the hexadecapole nonaxiality (but not the  $\beta_{60}$  and  $\beta_{80}$  terms) preserves the modulo- $60^\circ$  invariance in  $\gamma$ , so, in particular, the parameter  $\beta_{40}$  describes a deformation which is axially symmetric around the  $z$  axis at  $\gamma = 0^\circ$  and around the  $x$  axis at  $\gamma = 60^\circ$ , which allows to better approximate energy at oblate shapes. For this reason, while the original mesh Eq. (3) may be expected more reliable for barriers at small  $\gamma$ , the one of Eq. (8) is better for saddles closer to  $\gamma = 60^\circ$ , like those in nuclei with well- or super-deformed oblate ground states.

Our method of proceeding is analogous to that used in the study of the mass-asymmetry. The difference is that we do not have to perform the first step: a minimization with respect to  $\beta_{42}$  and  $\beta_{44}$  at the saddles found from the grid Eq. (3). Such calculations were already done in the previous studies of the effect of nonaxial deformations of higher multipolarity on the fission barrier in heaviest nuclei [46–49]. We know that the minimization gave the

largest effect in the following four regions of nuclei, see Fig. 2 in [49]: (I)  $Z \approx 122$ ,  $N \approx 160$  - up to 1.5 MeV, and a  $\sim 3$  times smaller effect for nuclei with larger  $N$  and  $Z > 120$ , (II)  $Z \approx 110$ ,  $N \approx 146$  - up to 1 MeV, (III)  $Z \approx 114$ ,  $N \approx 184$  - up to 1 MeV, and (IV)  $Z \approx 104$ ,  $N \approx 170$  - up to 0.4 MeV.

By applying the IWF method on the mesh Eq. (8) we have found the saddles for a dozen of nuclei from the last three regions, for which the effect of minimization was the largest. It turned out that, compared to saddles found on the original grid Eq. (3), they were lowered by less than 150 keV in the region (II), by less than 100 keV in the region (III), and even increased by  $\sim 100$  keV in the region (IV). On this basis we conclude that the lowering of the fission saddles found by the minimization in [7, 48] in these three regions is in a large measure a spurious effect which mostly vanishes when saddles are fixed by a proper method.

On the contrary, the substantial effect (up to  $\approx 1$  MeV) of the nonaxial hexadecapole in the region (I), although smaller than found by the minimization, survives in the exact IWF treatment. This might be expected as these are very heavy  $Z \geq 119$  nuclei with short barriers and oblate (also superdeformed) ground states, so  $\beta_{42}$  and  $\beta_{44}$  are necessary to reproduce energy in the vicinity of the oblate axis. Therefore, in the whole region of nuclei with  $Z \geq 118$  we calculated triaxial barriers by the IWF method using the mesh Eq. (8) and then selected the proper fission barriers from two 5D calculations.

Three types of saddles in nuclei from the region (I) are shown for a very heavy and exotic nucleus  $^{285}122$  in Fig. 8. The landscape was created from the 5D mesh Eq. (8).

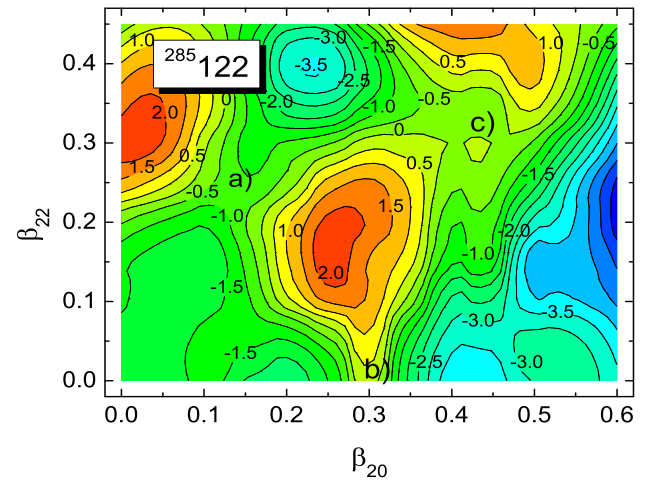


FIG. 8: Energy surface,  $E - E_{mac}(sphere)$ , for the nucleus  $Z = 122$ ,  $N = 163$ , resulting from the calculation according to Eq. (8).



This nucleus has a global superdeformed oblate (SDO) minimum with the quadrupole deformation  $\beta_{20} = -0.455$  (spheroid with the axis ratio  $\approx 3:2$ ). It represents a neutron-deficient area of superheavy nuclei according to recent predictions [50]. These intriguing SDO minima were already confirmed, as the global ones, by various self-consistent models [51, 52]. There is a saddle close to the oblate axis, separating the SDO g.s. from the wide minimum near the spherical shape - type a); the axially symmetric saddle is designated as b). One fission path may go through the saddles a) and b), the higher of which would define the barrier along this path. The second fission path goes through a triaxial saddle of type c) at  $\beta_{20} \approx 0.4$ ,  $\gamma \approx 35^\circ$ . The fission barrier of  $B_f = 3.6$  MeV corresponds to the saddle c) as found by using the grid Eq. (8). It turns out that saddles of type a) and c) are much lowered by including  $\beta_{42}$ ,  $\beta_{44}$ , the first usually more than the second.

Table II summarizes the effect of nonaxial hexadecapole on the barriers in the region (I). It contains 75 nuclei in which the barrier lowering is greater than 300 keV. The most frequent saddle type in the region (I), on both grids, is c), but there are also more complicated cases in which the saddle type changes when  $\beta_{42}$  and  $\beta_{44}$  are included. The largest effect of 1.167 MeV occurs in the nucleus  $Z = 125$ ,  $N = 163$ .

Let us remark that the difference between the results of the constrained minimization and the IWF method for the nonaxial hexadecapole is the main source of the discrepancy between the current fission barriers and those published in [7] for even-even nuclei.

#### D. Isotopic dependence

Calculated fission barriers given in Table III are illustrated along isotopic chains in Figures: 9 - 18. Generally, it can be seen that: i) in the whole region  $Z = 98 - 126$  the fission barrier heights are limited by:  $B_f \leq 8.06$  MeV; ii) there are characteristic maxima of fission barriers at  $Z \approx 100$ ,  $N \approx 150$ , near  $Z = 108$ ,  $N = 162$  (deformed magic shells) and  $Z = 114$ ,  $N = 178$  (not 184); high barriers occur also at the border of the studied region, for  $Z = 98$ ,  $N \approx 183$ ; iii) over intervals of  $N$  where  $B_f(N)$  increase or are on average constant, the fission barriers in a neighboring system  $N_{\text{even}} + 1$  are higher than  $B_f(N_{\text{even}})$ ; it may be the opposite over intervals where  $B_f(N)$  strongly decrease; the same behaviour can be seen when comparing barriers for isotones - see Fig. 20. This quite pronounced odd-even staggering in barriers is related to a decrease in the pairing gap due to blocking as it will be discussed in the next subsection.

In the isotopic dependence of the fission barriers for Cf, Es and Fm nuclei, shown in Fig. 9, there are two peaks of a similar size, at  $N = 152$  and  $N = 184$ . The minima of  $B_f(N)$  occur at  $N \approx 170$ . Odd-even staggering in  $B_f$  for Es is stronger around  $N = 152$ , while for Cf it is stronger near  $N = 184$ .

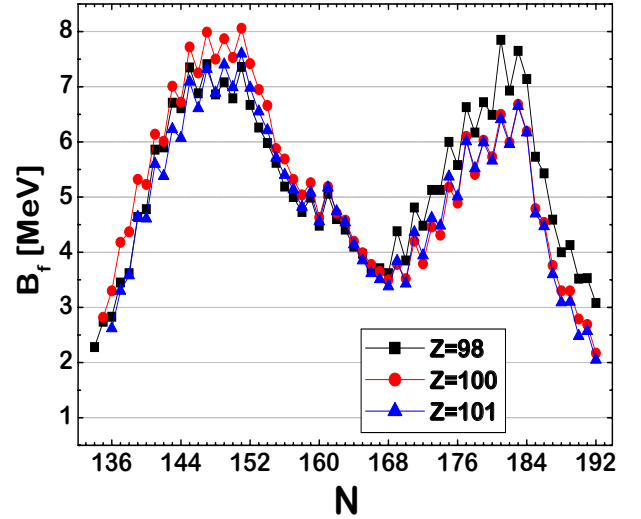


FIG. 9: Isotopic dependance of fission barriers for  $Z = 98, 99$  and  $Z = 100$ .

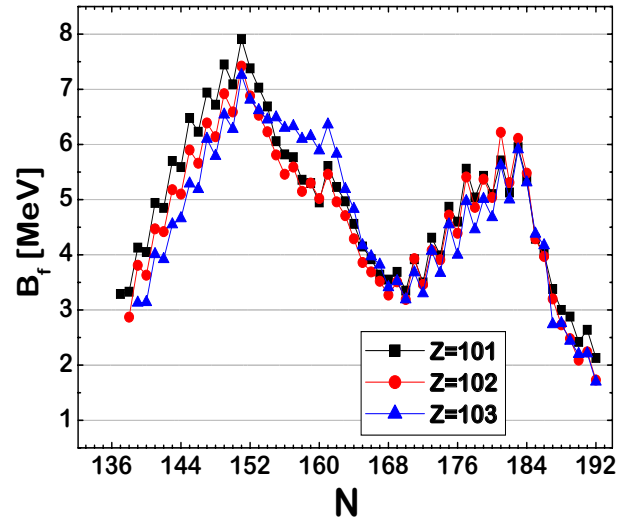


FIG. 10: The same as in Fig.9 but for  $Z = 101, 102$  and  $Z = 103$ .

For Md, No and Lr isotopes (Fig. 10), the second maximum around  $N = 184$  is weakening. A maximum associated with the semi-magic deformed shell at  $N = 162$  appears. As before, the minima of  $B_f(N)$  are located at  $N \approx 170$ . For Rf, Db, Sg, Bh and Hs nuclei (Fig. 11 and 12), previously distinct maximum at  $N = 152$  becomes more flat, and a kind of plateau forms between  $N = 152$  and 162. For Mt isotopes this plateau changes into a local minimum in the isotopic dependence  $B_f(N)$ , located

TABLE II: The barrier lowering (in MeV) greater than 0.3 MeV in nuclei  $Z \geq 118$ , in particular in those with SDO ground states, from the IWF calculations on the 5D mesh including  $\beta_{42}$  and  $\beta_{44}$  according to Eq. (8). Also reported is the associated change in the saddle type (for a description of saddle types see text); no entry means that a c-type saddle results from both grids, Eq. (3) and (8).

N	$\Delta B_f$	saddle	N	$\Delta B_f$	saddle	N	$\Delta B_f$	saddle
<b>Z = 119</b>			<b>Z = 122</b>			<b>Z = 125</b>		
155	0.597		158	0.779		161	1.083	
156	0.482		159	0.959		162	0.958	
157	0.472		160	0.807		163	1.167	
158	0.566		161	0.731		164	0.936	
159	0.585		162	0.690		165	0.439	a→c
160	0.508		163	0.469	a→c	166	0.806	b→c
161	0.315	b→c	164	0.364	b→c	167	0.806	
162	0.471	a→c	169	0.403	b→c	168	0.800	
170	0.343	b→c	170	0.365		169	0.714	
172	0.480	b→c	<b>Z = 123</b>			170	0.551	
173	0.501		159	0.831		<b>Z = 126</b>		
174	0.400		160	0.821		162	0.995	
<b>Z = 120</b>			161	0.863		163	1.099	
156	0.613		162	0.924		164	1.034	
157	0.731		163	0.496	a→c	165	0.802	
158	0.652		164	0.480	a→c	166	0.912	
159	0.778		168	0.357	b→c	167	0.807	
160	0.696		169	0.300	b→c	168	0.845	
161	0.658		<b>Z = 124</b>			169	0.911	
162	0.581	a→c	160	0.819		170	0.735	
163	0.323	a→b	161	0.868		171	0.534	
<b>Z = 121</b>			162	0.896		172	0.434	
157	0.747		163	0.741				
158	0.774		164	0.739	a→c			
159	0.690		165	0.333	b→c			
160	0.830		166	0.334	b→c			
161	0.688		167	0.455	b→c			
162	0.633	b→c	168	0.519	b→c			
			169	0.459				
			170	0.328				

around  $N=155$ . The highest barriers in Bh, Hs and Mt isotopic sets occur at  $N \approx 162$ .

For Ds, Rg and Cn nuclei (Fig. 13), with the increasing proton number the  $N=184$  spherical shell starts to dominate. However, not much lower barriers are obtained near the deformed gap  $N=162$ .

For nuclei:  $Z = \text{Nh, Fl, Mc}$  (Fig. 14), one can see one region with high barriers, around  $N=180$ . One can notice that the maxima in  $B_f(N)$  are already shifted toward  $N < 184$ . Slight residues of the formerly observed shells at  $N=152$  and  $N=162$  can be spotted.

For nuclei:  $Z = \text{Lv, Ts, Og}$  (Fig. 15), the main maximum in  $B_f$  progresses further towards smaller  $N$ , reaching finally  $N \approx 175$ . The minima in  $B_f(N)$ , observed

before at  $N = 172$ , gradually disappear. For nuclei:  $Z=119, Z=120, Z=121$  (Fig. 16), the situation is similar to that described above. Barriers in nuclei  $Z=122, 123, 124$  (Fig. 17), compared to the previous set, are clearly lower. The maximum is even more shifted towards smaller  $N$ . For nuclei:  $Z=125, 126$  (Fig. 18) the fission barriers are still lower. Their maxima occur at  $N=171$  and  $173$ .

All calculated fission barriers heights are collected together and shown as a map  $B_f(Z, N)$  in Fig. 19. One can see three areas with clearly raised barriers: around  $N \approx 152$ ,  $N=162$  and  $N \approx 180$ , and the region of low barriers around  $N=170$ , as discussed above. The effect of the odd particle, i.e. an often (but not always) higher

barrier in a neighboring odd-particle system can be also seen in Fig. 19.

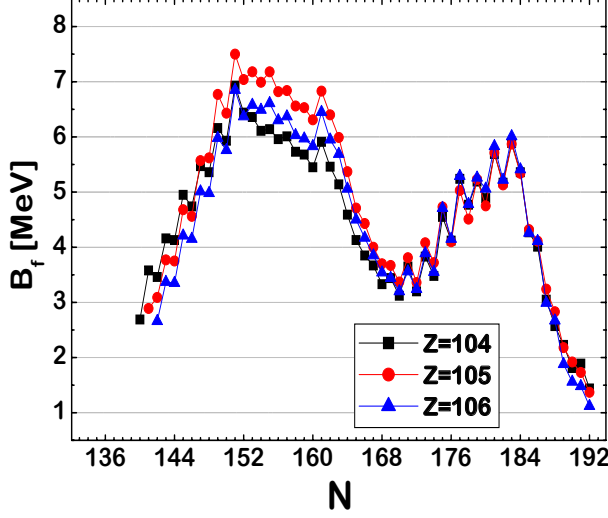


FIG. 11: The same as in Fig.9 but for  $Z = 104, 105$  and  $Z = 106$ .

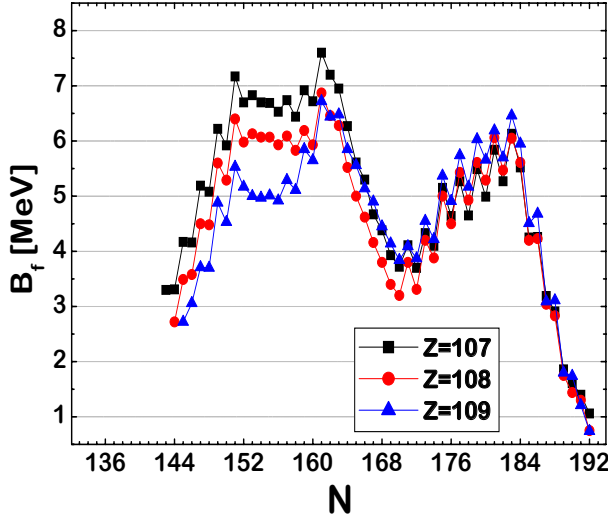


FIG. 12: The same as in Fig.9 but for  $Z = 107, 108$  and  $Z = 109$ .

### E. Role of the pairing interaction and the odd-even barrier staggering

It is known that the blocking procedure often causes an excessive reduction of the pairing gap in systems with an odd particle number. This effect is much more pronounced in the g.s. than in the fission saddle, as the pairing gap is never small in the latter. One device to avoid an excessive even-odd staggering in nuclear binding was to assume a stronger (typically by  $\sim 5\%$ ) pairing

interaction for odd-particle-number systems, see [41–44]. Here, instead of performing another grid calculation with modified pairing strengths, we tested the magnitude of their effect on fission barriers by increasing them by 5 and 10 percent for odd particle numbers (neutrons or protons) at previously found ground states and saddle points. The results of this test are presented in Fig. 20 for the  $N=169$  isotones and in Fig. 21 for the  $Z=109$  isotopic chain.

Both the isotopic and isotonic dependence show that

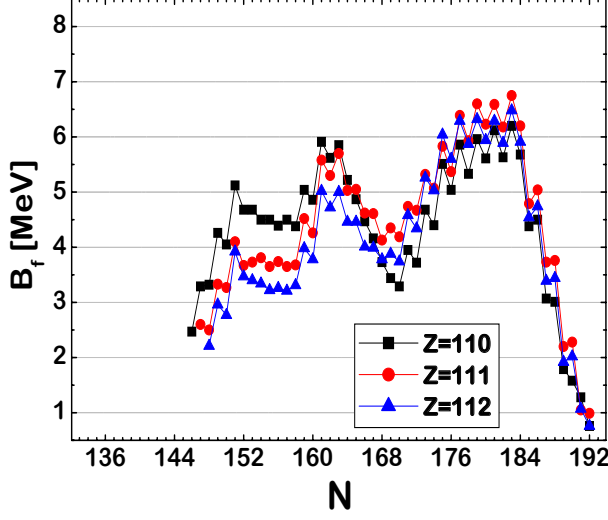


FIG. 13: The same as in Fig.9 but for  $Z = 110, 111$  and  $Z = 112$ .

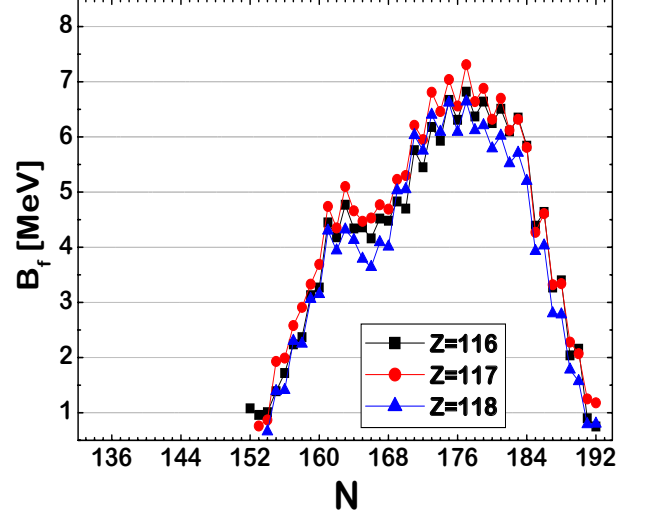


FIG. 15: The same as in Fig.9 but for  $Z = 116, 117$  and  $Z = 118$ .

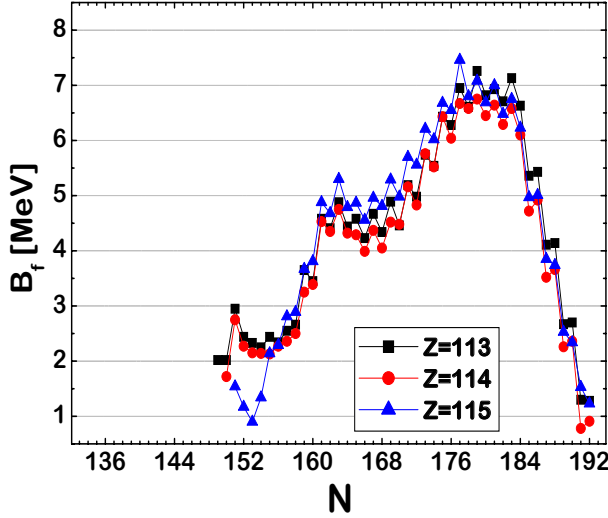


FIG. 14: The same as in Fig.9 but for  $Z = 113, 114$  and  $Z = 115$ .

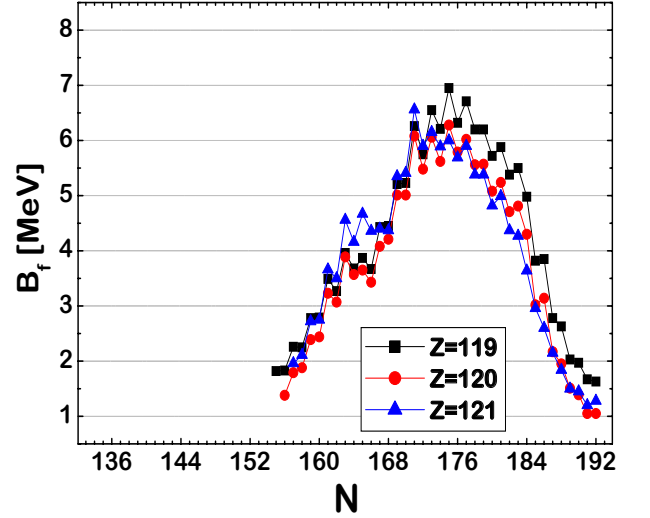


FIG. 16: The same as in Fig.9 but for  $Z = 119, 120$  and  $Z = 121$ .

increasing the intensity of pairing leads to a reduction of the fission barrier by a variable amount. When the pairing strengths are increased by 5% for odd particle numbers, the fission barriers decrease in odd-even, even-odd and odd-odd systems by up to 0.5 MeV; the 10% increase in the pairing strengths can decrease the barriers at most by about 1 MeV. The same pairing change leads to the suppression, and then the inversion of the staggering effect.

The even-odd barrier staggering related to pairing is convoluted with the isotopic or isotonic dependence related to the mean-field. With the original pairing, when one separates a linear part of the latter by calculating:  $B_f(Z_{\text{odd}}, N) - 1/2[B_f(Z_{\text{odd}} + 1, N) + B_f(Z_{\text{odd}} - 1, N)]$ , and an analogous quantity for odd neutron numbers, one obtains numbers between 1.053 and  $-0.947$  MeV, with the average of  $\approx 0.22$  MeV for protons and  $\approx 0.26$  MeV for neutrons. As shown by black points in Fig. 20, 21,

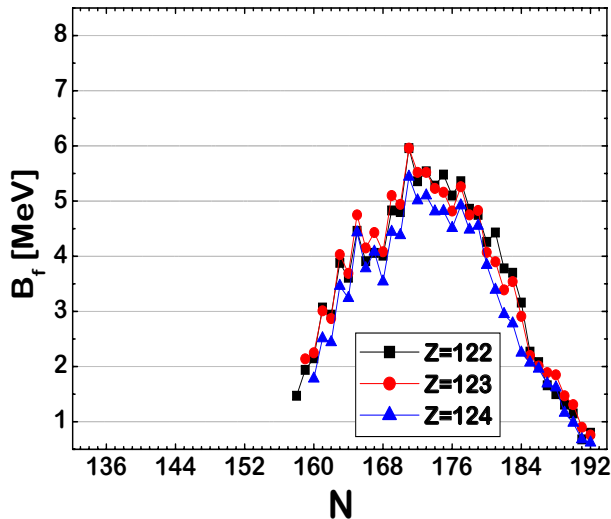


FIG. 17: The same as in Fig.9 but for  $Z = 122, 123$  and  $Z = 124$ .

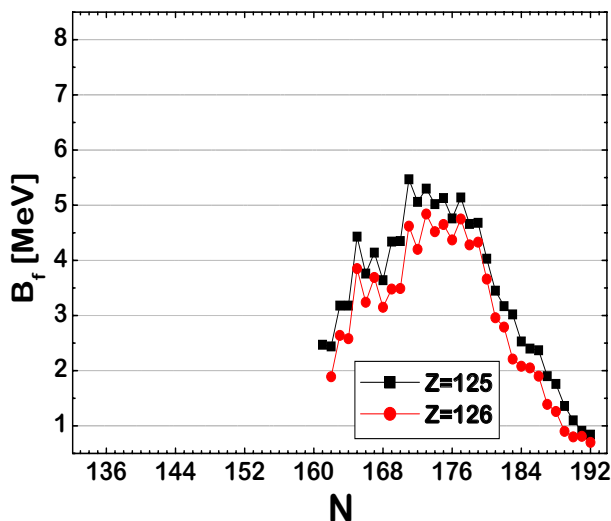


FIG. 18: The same as in Fig.9 but for  $Z = 125$  and  $Z = 126$ .

the effect is indeed irregular and, when present, typically at the level of several hundred keV.

The 5% increase in pairing for odd particle numbers reduces the staggering in  $N = 169$  isotones and nearly cancels it in  $Z = 109$  isotopes (red points in Fig.20 and 21). The important point is that the 10% increase in pairing for odd number of particles *inverts* the staggering, at least locally: near  $Z = 120$  in  $N = 169$  isotones and near  $N = 153$ ,  $N = 162$  and  $N = 180$  in Mt isotopes (green points in Fig.20 and 21).

Although the spontaneous fission rates of odd-particle number nuclei are smaller by 3-5 orders of magnitude than those of their even neighbors, the experimental fission barriers in actinides show only a moderate odd-even staggering, c.f. [53, 54]. Still, it is inconceivable that the fission barriers in odd- $Z$  or odd- $N$  systems should be on average *smaller* than in their even neighbors. This indicates that the 10% increase in pairing strengths in odd- $N$  or odd- $Z$  systems would be too large. A qualitative argument which follows is that even if the blocking method overestimates the pairing decrease, the fission barriers of odd- $Z$  or/and odd- $N$  nuclei should fall in a strip between the black and red points in Fig.20 and 21. Thus, the test of the pairing influence on barriers points that a possible overestimate of barriers in odd- $A$  and odd-odd nuclei, induced by the blocking, should not be much larger than 0.5 MeV. One may add in this context that the barriers from the FRLDM model do not show any even-odd staggering due to the way the pairing was included there.

#### F. Comparison with other theoretical calculations and some empirical data

Let us discuss the results in Table III in relation to available empirical data and to the other theoretical estimates.

As an empirical check of our model, one can use the barriers in the actinide region. We have reported quite a spectacular agreement of the calculated first [7] and second [8] fission barriers in even-even actinides with the data [53, 54], with root mean square deviation 0.5 MeV and 0.7 MeV, respectively.

The heaviest nucleus in which the fission barrier height has been measured recently is  $^{254}\text{No}$ . The value  $B_f = 6.0 \pm 0.5$  MeV at spin  $15\hbar$ , giving by extrapolation  $B_f = 6.6 \pm 0.9$  MeV at the spin  $0\hbar$ , has been deduced from the measured distribution of entry points in the excitation energy vs. angular momentum plane [55]. This result perfectly agrees with our evaluation:  $B_f = 6.88$  MeV (at spin  $0\hbar$ ) and with the MM model [64] which gives:  $B_f = 6.76$  MeV. The selfconsistent calculations, mainly based on the Skyrme interaction, overestimate this barrier significantly [56–58] (9.6 and 8.6 or 12.5 MeV, respectively). There are experimental estimates of barriers in a few SH nuclei, based on observed ER production probabilities [61], which again well agree with our barriers, see [7]. Apart from those, fission barriers in the SH region are generally unknown.

As a supplementary insight, one can crosscheck barriers evaluated within various models. Quite recently we noted a dramatic divergence in calculated fission barriers [59]. Since, as it was discussed previously, the inclusion of triaxiality is absolutely necessary in the SH region, we have chosen only models which take this into account. In fact, there is only one systematic calculation, including triaxiality and odd-particle-number nuclei - the Finite Range Liquid Drop Model [13, 60, 64]

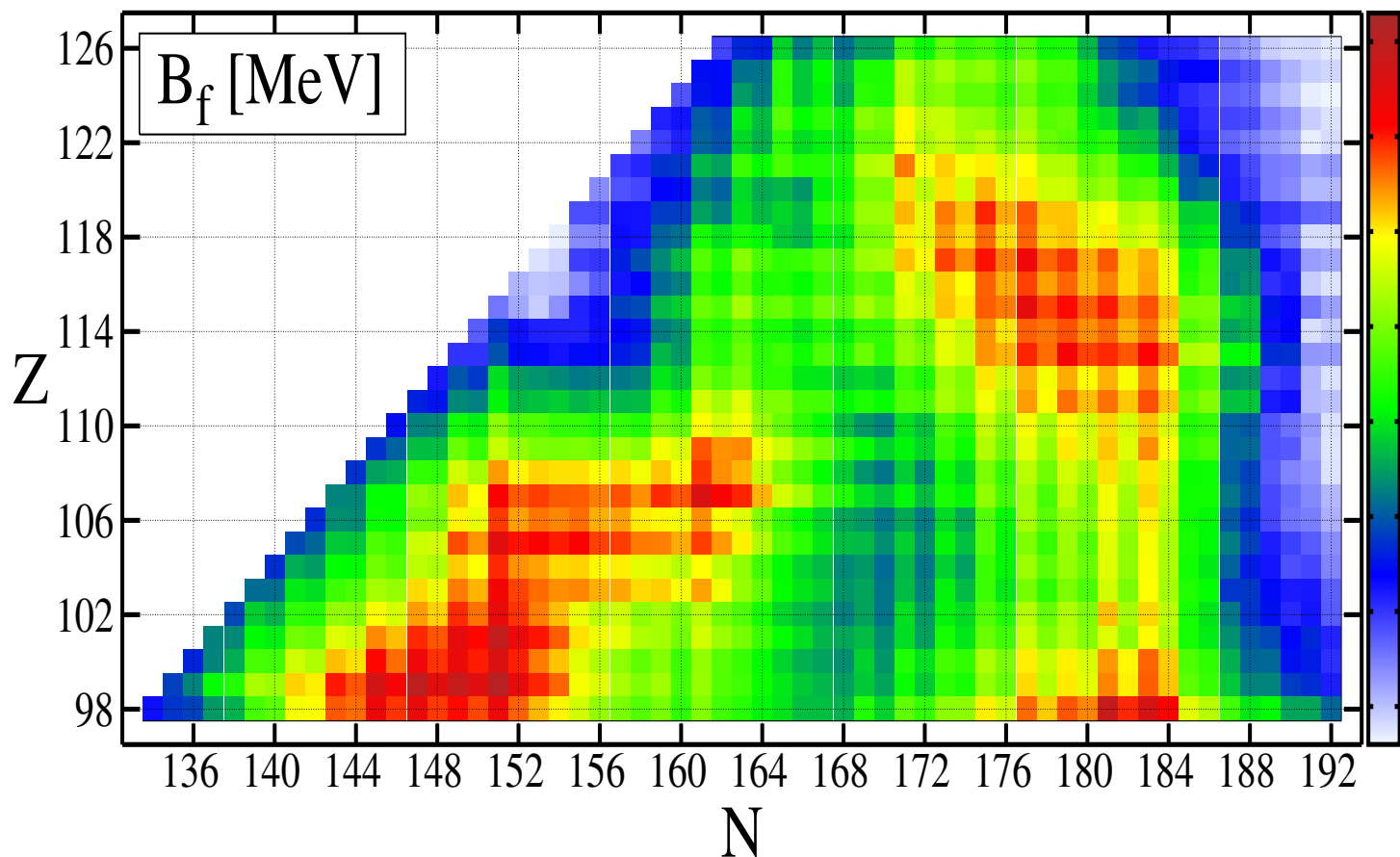


FIG. 19: Calculated fission barrier heights  $B_f$  for superheavy nuclei.

(FRLDM) developed by Los Alamos group. It can be noted though, that the inner fission barrier is fixed there in only three-dimensional deformation space, what is certainly not enough.

The first conclusion from the comparison between our results and those of FRLDM is that a conspicuous barrier staggering between odd- and even-particle number nuclei is obtained in the Woods-Saxon model. As mentioned before, this results from the blocking treatment of pairing. At present it is not certain how large this staggering should be.

One can include more models for comparison if one confines it to even - even nuclei. We take the covariant density functional model [63] with the nonlinear meson-nucleon coupling, represented by the NL3\* parametrization of the relativistic mean-field (RMF) Lagrangian and the Hartree-Fock-Bogoliubov (HFB) approach with the SkM\* Skyrme energy density functional [62].

As can be seen in Fig. 22, fission barriers in Hassium nuclei are quite similar in all models. The values of  $B_f$  differ up to 2 MeV, but never more. Regarded as a func-

tion of  $N$ , they show a maximum close to the semi-magic number  $N=162$  while the second maximum is related with the  $N=184$  spherical gap. In the FRLDM this maximum is barely outlined and slightly shifted to the neutron deficient side. The minimum in barriers is obtained in both MM models at the similar place ( $N=170$ ), while the RMF gives the smallest barriers at  $Z=174$ .

As one can see in Fig. 23, for Flerovium isotopes the barriers calculated here are in agreement with the experimental (empirical) estimates [61] and with the self-consistent calculations [62] based on the SKM\* interaction. The FRLDM [64] overestimates these quasi-empirical barriers [61] significantly. Although only the lower limit for the barrier height has been estimated in [61], which would reproduce the known cross sections on the picobarn level, such a high barrier seems problematic, see discussion in [65, 66]. On the other hand, with extremely small barriers obtained within the RMF model one cannot explain experimentally known millisecond fission half-life in  $^{284}\text{Fl}$ . One should note, however, that a slight tuning of the RMF model [67] gives higher barriers,

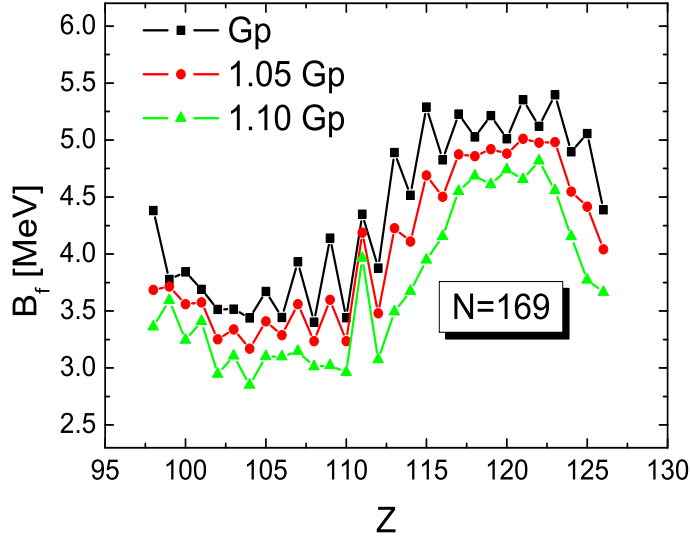


FIG. 20: Effect of the pairing strength increase (while keeping fixed the g.s. and saddle deformations) in  $N=169$  isotones: standard  $G_n$  and  $G_p$  - black points,  $G_n$  and  $G_p$  increased by 5% (10%) for odd- $Z$  and odd- $N$  nuclei - red (green) points.

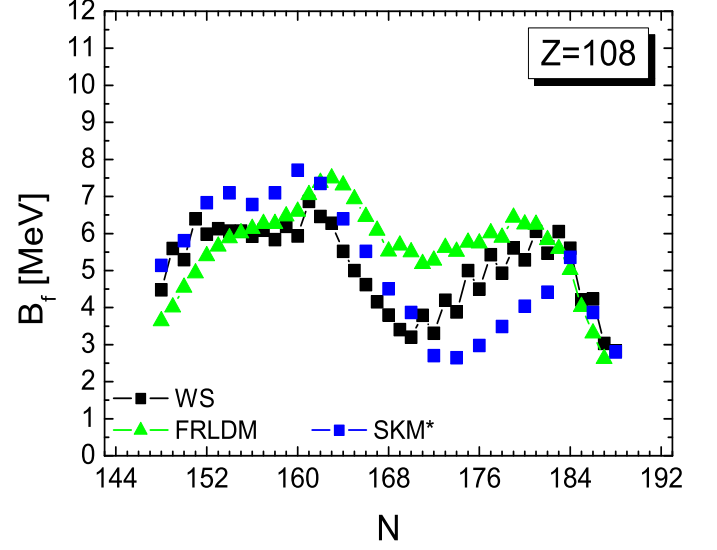


FIG. 22: Fission barriers predicted by various models for Hassium isotopes: black - WS model, green FRLDM [64], blue SKM\* [62], red RMF with NL3 parametrization [63]. Experimental data taken from [61]. (For interpretation of the references to color in this figure legend, the reader is referred to the web version of this article.)

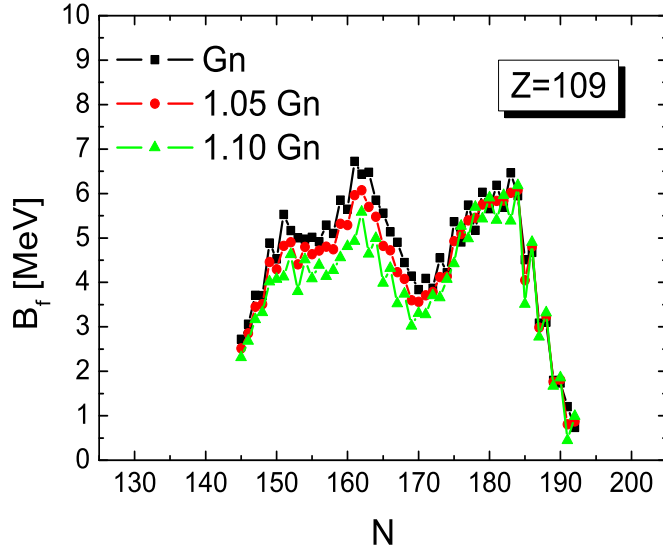


FIG. 21: Effect of the pairing strength increase (while keeping fixed the g.s. and saddle deformations) in  $Z=109$  isotopes: standard  $G_n$  and  $G_p$  - black points,  $G_n$  and  $G_p$  increased by 5% (10%) for odd- $Z$  and odd- $N$  nuclei - red (green) points.

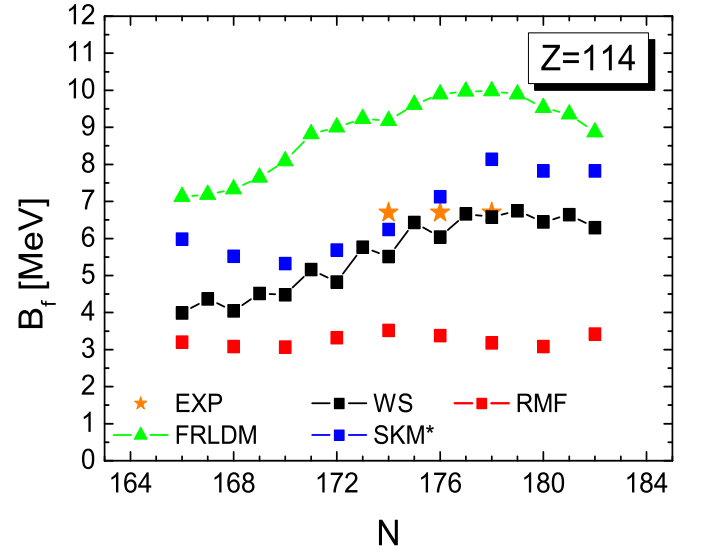


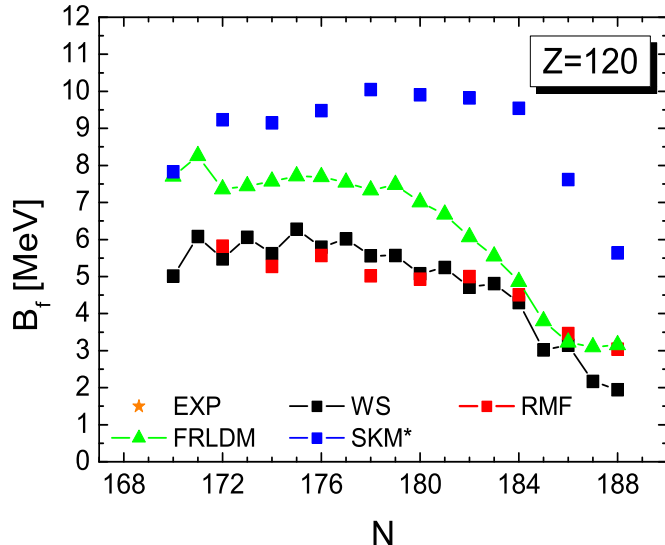
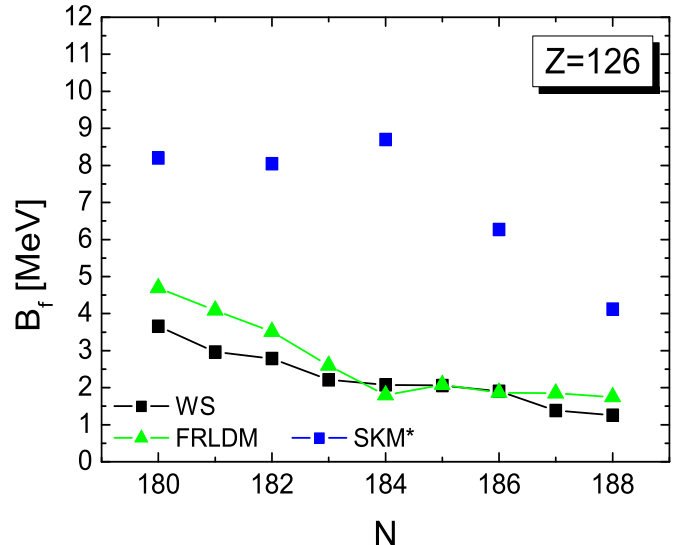
FIG. 23: The same as in Fig 22 but for  $Z=114$ .

thus, closer to ours. This is true, especially in Cn and Fl isotopes, see details in Fig. 5 in [67] and discussion

included there.

For  $Z=120$  our results, shown in Fig. 24, are very



FIG. 24: The same as in Fig 22 but for  $Z=120$ .FIG. 25: The same as in Fig 22 but for  $Z=126$ .

#### IV. CONCLUSIONS

close to those obtained within the RMF model. The results of [64] are systematically higher by  $\approx 1$  MeV. This is in an evident contrast with the Skyrme SkM\* prediction [62] of the highest barriers for  $Z = 120$  [62] - related to the proton magic gap. Three models: FRLDM, RMF and ours converge at  $N=182-184$  to  $B_f \simeq 5$  MeV. The nucleus  $^{302}120$  is particularly interesting, as two unsuccessful attempts to produce it have already taken place in GSI, providing a cross-section limit of 560 fb [68] or 90 fb in [69], and in Dubna [70], providing the limit of 400 fb. The cross-section estimates [71] do not support a possibility of an easy production of this SH isotope in the laboratory. It seems that with the barrier of the order of 10 MeV, as obtained in the frame of the self-consistent theory, producing superheavy  $Z=120$  nuclei should not pose any difficulties.

In the case of  $Z=126$ , shown in Fig. 25, both MM models give significantly smaller barriers than the model based on the SKM\* force. For example, the barrier  $B_f \approx 9$  MeV for  $^{310}126$ , calculated with this Skyrme interaction, is still impressively large. This might induce thoughts on the ways of synthesis of such superheavy systems, but one has to remember that the predicted half-lives with respect to  $\alpha$  decay are below the present-day  $10^{-5}$  s time-limit for the experimental identification. On the contrary,  $B_f \approx 2$  MeV obtained in the MM approach does not induce any hopes; it only points to a quite striking disagreement between models.

We have determined fission barriers for 1305 heavy and superheavy nuclei, including odd- $A$  and odd-odd systems, within the macroscopic-microscopic method by following the adiabatic configuration in each nucleus. The applied Woods-Saxon model was widely used for heavy nuclei and well reproduces experimental fission barriers in actinides. For odd- $Z$  or/and odd- $N$  nuclei pairing was included within the blocking procedure. Triaxial and mass-asymmetric deformations were included and the IWF method used for finding the saddles which allowed to escape errors inherent in the constrained minimization approach. To find saddles, energy for each nucleus was calculated on a 5D deformation grid and then 5-fold interpolated in each dimension for the IWF search. Two additional energy grids: a second 5D and another 7D, were calculated in order to include nonaxial hexadecapole and mass-asymmetry effects on fission barriers. The following conclusions can be drawn from our investigation:

i) Global calculations confirm the existence of two physically important areas in the  $Z$ - $N$  plane with prominent barriers: one located around the semi-magic quantum numbers  $Z = 100 - 108$  and  $N = 150 - 162$  (connected with deformed closed shells) and the second - of nearly spherical nuclei around  $Z = 114$  and  $N = 176 - 180$ . The highest fission barrier among the studied nuclei occurs in very exotic  $\text{Es}^{250}$ .

ii) The well-known effect of the mass asymmetry on the second barrier in actinides is not very relevant for the heaviest nuclei since very deformed barriers at  $\beta_{20} \approx 0.8$

decrease with increasing  $Z$  and fission barriers are fixed by the less deformed saddles. However, in some nuclei with  $Z \geq 109$  the mass(reflection) asymmetry effect lowers the first saddles which are sometimes split into two humps. It seems that this concerns only axially-symmetric saddles. The largest barrier lowering (by 0.8 MeV) has been observed for  $Z = 113$  and  $N = 157$ .

iii) It has been demonstrated that the inclusion of triaxial shapes significantly reduces the fission barriers by up to 2.5 MeV; about 70% of the found fission barriers correspond to triaxial saddles. Besides the quadrupole nonaxiality we checked also the effect of hexadecapole nonaxiality which significantly lowers the fission barrier in  $Z \geq 119$  nuclei, especially neutron-deficient ones.

iv) Rather strong, irregular odd-even  $Z$  or  $N$  barrier staggering effect resulted from the blocking formalism used for pairing. The barrier of an odd nucleus  $Z_{\text{even}} + 1$  or  $N_{\text{even}} + 1$  is typically by several hundred keV higher than that of its even neighbor.

v) The existing theoretical evaluations of fission barriers

differ significantly. Even the results of the two models based on the microscopic-macroscopic approach differ dramatically for some nuclei. Our calculations indicate, in contrast to the self-consistent mean-field studies, that fission barriers, still quite substantial for some  $Z = 118$  nuclei, become lower than 5.5 MeV for  $Z = 126$ .

## V. ACKNOWLEDGMENT

M.K. and J.S. were co-financed by the National Science Centre under Contract No. UMO-2013/08/M/ST2/00257 (LEA COPIGAL). One of the authors (P.J.) was cofinanced by Ministry of Science and Higher Education: Iuventus Plus grant Nr IP2014 016073. This research was also supported by an allocation of advanced computing resources provided by the Swierk Computing Centre (CIS) at the National Centre for Nuclear Research (NCBJ) (<http://www.cis.gov.pl>).

- 
- [1] J. H. van't Hoff, "Etudes de Dynamiques Chimiques" (F. Muller & Co., Amsterdam, 1884), p. 115
  - [2] S. Arrhenius, *Z. Phys. Chem.* **4**, 226 (1889)
  - [3] Yu.Ts. Oganessian, V.K. Utyonkov., *Nucl. Phys. A* **944** (2015).
  - [4] P. Jachimowicz, M. Kowal, and J. Skalski, *Phys. Rev. C*, **92**, 044306 (2015).
  - [5] S. Goriely, M. Samyn, and J.M. Pearson, *Phys. Rev. C* **75**, 064312 (2007).
  - [6] A. Baran, M. Kowal, P. -G. Reinhard, L. M. Robledo, A. Staszczak, M. Warda, *Nucl. Phys. A* **944**, (2015).
  - [7] M. Kowal, P. Jachimowicz, A. Sobiczewski, *Phys. Rev. C* **82**, 014303 (2010).
  - [8] P. Jachimowicz, M. Kowal, J. Skalski *Phys. Rev. C*, **85**, 034305 (2012).
  - [9] M. Kowal, J. Skalski *Phys. Rev. C* **82**, 054303 (2010).
  - [10] M. Kowal, J. Skalski *Phys. Rev. C* **85**, 061302(R) (2012).
  - [11] P. Jachimowicz, M. Kowal, J. Skalski *Phys. Rev. C*, **88**, 044308 (2013).
  - [12] P. Jachimowicz, M. Kowal, and J. Skalski, *Phys. Rev. C*, **89**, 024304 (2014).
  - [13] P. Möller et al., *Phys. Rev. C* **79**, 064304 (2009).
  - [14] N. Dubray, and D. Regnier, *Comp. Phys. Comm.* **183**, 2035 (2012)
  - [15] N. Schunck, D. Duke, H. Carr, and A. Knoll, *Phys. Rev. C* **90**, 054305 (2014).
  - [16] W. Brodzinski and J. Skalski, *Phys. Rev. C* **88**, 044307 (2013).
  - [17] S. Ćwiok, J. Dudek, W. Nazarewicz, J. Skalski and T. Werner, *Comput. Phys. Commun.* **46**, 379 (1987).
  - [18] V. M. Strutinski, *Sov. J. Nucl. Phys.* **3**, 449 (1966), *Nucl. Phys. A* **95**, 420 (1967).
  - [19] H. J. Krappe, J. R. Nix and A. J. Sierk, *Phys. Rev. C* **20**, 992 (1979).
  - [20] I. Muntian, Z. Patyk and A. Sobiczewski, *Acta Phys. Pol. B* **32**, 691 (2001).
  - [21] P. Möller and A. Iwamoto *Phys. Rev. C* **61**, 047602 (2000).
  - [22] V. Luc and P. Soille, *IEEE Trans. Pattern Anal. Mach. Intell.*, **13**, 583 (1991).
  - [23] A. Mamdouh, J.M. Pearson, M. Rayet, and F. Tondeur, *Nucl. Phys. A* **644**, 389 (1998).
  - [24] B. Hayes, *Am. Sci.* **88**, 481 (2000).
  - [25] P. Möller, A. J. Sierk and A. Iwamoto, *Phys. Rev. Lett.* **92**, 072501 (2004).
  - [26] Z. Patyk, A. Sobiczewski, P. Armbruster, and K.-H. Schmidt, *Nucl. Phys. A* **491**, 267 (1989).
  - [27] Z. Patyk and A. Sobiczewski, *Nucl. Phys. A* **533**, 132 (1991).
  - [28] Z. Patyk and A. Sobiczewski, *Phys. Lett. B* **256**, 307 (1991).
  - [29] R. Smolaczuk, J. Skalski, and A. Sobiczewski, *Phys. Rev. C* **52**, 1871 (1995).
  - [30] Bing-Nan Lu, Jie Zhao, En-Guang Zhao, and Shan-Gui Zhou, *Phys. Rev. C* **89**, 014323 (2014).
  - [31] S. Ćwiok and A. Sobiczewski, *Z. Phys. A* **342**, (1992).
  - [32] S. Ćwiok et al., *Phys. Lett. B* **322**, 304 (1994).
  - [33] S. Ćwiok, J. Dobaczewski, P. -H. Heenen, P. Magierski, and W. Nazarewicz, *Nucl. Phys. A* **611**, 211 (1996).
  - [34] R. A. Gherghescu, J. Skalski, Z. Patyk and A. Sobiczewski, *Nucl. Phys. A* **651**, (1999).
  - [35] J. Dechargé, J.F. Berger, M. Girod, and K. Dietrich, *Nucl. Phys. A* **716**, 55 (2003).
  - [36] A. K. Dutta, J. M. Pearson, F. Tondeur, *Phys. Rev. C* **61**, 054303 (2000).
  - [37] L. Bonneau, P. Quentin and D. Samsoen, *Eur. Phys. J. A* **21**, 391 (2004).
  - [38] S. Ćwiok, P.-H. Heenen, W. Nazarewicz, *Nature* **433**, 709 (2005).
  - [39] A. Dobrowolski, K. Pomorski, J. Bartel, *Phys. Rev. C* **75**, 024613 (2007).
  - [40] M. Kowal, A. Sobiczewski, *Int. J. Mod. Phys. E* **18**, 4, 914, (2009).
  - [41] F. Tondeur, S. Goriely, J. M. Pearson and M. Onsi, *Phys. Rev. C* **62**, 024308 (2000).

- [42] F. Tondeur, S. Goriely, J. M. Pearson and M. Onsi, *Phys. Rev. C* **66**, 024326 (2002).
- [43] F. Tondeur, S. Goriely, J. M. Pearson and M. Onsi, *Phys. Rev. C* **68**, 054325 (2003).
- [44] F. Tondeur, S. Goriely, J. M. Pearson and M. Onsi, *Phys. Rev. C* **70**, 044309 (2004).
- [45] R. W. Hasse, W. D. Myers, "Geometrical Relationships of Macroscopic Nuclear Physics." *Springer-Verlag Berlin Heidelberg*, (1988).
- [46] A. Sobczewski, L. Shvedov, M. Kowal, *Int. J. Mod. Phys. E* **16**, 402 (2007).
- [47] M. Kowal and A. Sobczewski, *Int. J. Mod. Phys. E* **16**, 425 (2007).
- [48] M. Kowal and A. Sobczewski, *Int. J. Mod. Phys. E* **18**, 914 (2009).
- [49] A. Sobczewski, P. Jachimowicz, M. Kowal *Int. J. Mod. Phys. E* **19**, 493 (2010).
- [50] P. Jachimowicz, M. Kowal, and J. Skalski, *Phys. Rev. C* **83**, 054302 (2011).
- [51] L. Prochniak, A. Staszczak, *Acta Physica Polonica B***44**, 287 (2013).
- [52] P.-H. Heenen, J. Skalski, A. Staszczak, D. Vretenar, *Nucl. Phys. A* **944**, (2015).
- [53] G. N. Smirenkin, IAEA Report INDC(CCP)-359, Vienna (1993), <http://www-nds.iaea.org/RIPL-3/>
- [54] A. Mamdouh, J.M. Pearson, M. Rayet, and F. Tondeur, *Nucl. Phys. A* **644**, 389 (1998), <http://www-nds.iaea.org/RIPL-2/>
- [55] Greg Henning et al., *Phys. Rev. Lett.* **113**, 262505 (2014).
- [56] L. Bonneau, P. Quentin, and D. Samsen, *Eur. Phys. J. A* **21**, 391 (2004).
- [57] T. Duguet, P. Bonche, and P.-H. Heenen, *Nucl. Phys. A***679**, 427 (2001).
- [58] A. Staszczak, J. Dobaczewski, W. Nazarewicz, *IJMP*, **15**, No. 2 (2006).
- [59] W. Brodzinski, P. Jachimowicz, M. Kowal, J. Skalski, *Japan Phys. Soc. Conf. Proceedings Vol. 6*, 020054 (2015).
- [60] P. Möller, J.R. Nix, W.D. Myers and W.J. Świątecki, *At. Data Nucl. Data Tables* **59** (1995) 185.
- [61] M.G. Itkis, Y.T. Oganessian, V.I. Zagrebaev, *Phys. Rev. C*, **65**, 044602 (2002).
- [62] A. Staszczak, A. Baran, and W. Nazarewicz: *Phys. Rev. C* **87** (2013) 024320.
- [63] H. Abusara, A. V. Afanasjev, and P. Ring: *Phys. Rev. C* **85** (2012) 024314; **C 82** (2010) 044303.
- [64] P. Moller, A. J. Sierk, T. Ichikawa, A. Iwamoto, and M. Mumpower, *Phys. Rev. C* **91**, 024310 (2015).
- [65] K. Siwek-Wilczyńska, T. Cap, M. Kowal, A. Sobczewski and J. Wilczyński, *Phys. Rev. C*, **86**, 014611 (2012).
- [66] K. Siwek-Wilczyńska, T. Cap, M. Kowal and J. Wilczyński, *Physica Scripta*, **T154** (2013).
- [67] A.V. Afanasjev, S.E. Agbemava, *Acta Physica Polonica*, **B 46**, (2015).
- [68] S. Hofmann et al., *GSI Sci. Rep.*, p. 205 (2015).
- [69] S. Hofmann, *Russ. Chem. Rev.* **78**, 1123 (2009).
- [70] Oganessian, Yu.Ts. Utyonkov, V. Lobanov, Yu. Abdullin, F. Polyakov, A. Sagaidak, R. Shirokovsky, I. Tsyganov, Yu. et al. (2009). *Phys. Rev. C* **79** (2) (2009).
- [71] K. Siwek-Wilczyńska, T. Cap, and J. Wilczyński, *Int. J. Mod. Phys. , E***19**,500 (2010).

TABLE III: Calculated fission barrier heights (in MeV).

N	A	$B_f$	N	A	$B_f$	N	A	$B_f$	N	A	$B_f$	N	A	$B_f$
<b>Z=98</b>			<b>Z=99</b>			<b>Z=100</b>			<b>Z=101</b>			<b>Z=102</b>		
134	232	2.28												
135	233	2.74												
136	234	2.83	135	234	2.82									
137	235	3.45	137	235	3.30	136	236	2.62						
138	236	3.62	137	236	4.18	137	237	3.30	137	238	3.29			
139	237	4.64	138	237	4.37	138	238	3.58	138	239	3.33	138	240	2.87
140	238	4.78	139	238	5.32	139	239	4.64	139	240	4.13	139	241	3.81
141	239	5.86	140	239	5.23	140	240	4.61	140	241	4.05	140	242	3.63
142	240	5.90	141	240	6.14	141	241	5.60	141	242	4.94	141	243	4.47
143	241	6.71	142	241	6.01	142	242	5.38	142	243	4.85	142	244	4.42
144	242	6.61	143	242	7.01	143	243	6.23	143	244	5.70	143	245	5.18
145	243	7.35	144	243	6.72	144	244	6.07	144	245	5.59	144	246	5.10
146	244	6.88	145	244	7.72	145	245	7.09	145	246	6.48	145	247	5.90
147	245	7.41	146	245	7.25	146	246	6.61	146	247	6.23	146	248	5.66
148	246	6.86	147	246	7.99	147	247	7.32	147	248	6.94	147	249	6.39
149	247	7.08	148	247	7.50	148	248	6.89	148	249	6.72	148	250	6.14
150	248	6.79	149	248	7.87	149	249	7.40	149	250	7.45	149	251	6.92
151	249	7.36	150	249	7.53	150	250	6.99	150	251	7.09	150	252	6.59
152	250	6.67	151	250	8.06	151	251	7.60	151	252	7.91	151	253	7.42
153	251	6.26	152	251	7.42	152	252	6.98	152	253	7.38	152	254	6.88
154	252	5.98	153	252	6.95	153	253	6.55	153	254	7.03	153	255	6.53
155	253	5.62	154	253	6.66	154	254	6.21	154	255	6.69	154	256	6.23
156	254	5.19	155	254	5.88	155	255	5.71	155	256	6.06	155	257	5.81
157	255	5.00	156	255	5.69	156	256	5.40	156	257	5.82	156	258	5.46
158	256	4.73	157	256	5.32	157	257	5.14	157	258	5.77	157	259	5.59
159	257	4.99	158	257	5.04	158	258	4.82	158	259	5.36	158	260	5.15
160	258	4.48	159	258	5.26	159	259	5.08	159	260	5.30	159	261	5.30
161	259	5.06	160	259	4.63	160	260	4.56	160	261	4.95	160	262	5.02
162	260	4.60	161	260	5.19	161	261	5.17	161	262	5.61	161	263	5.46
163	261	4.41	162	261	4.71	162	262	4.74	162	263	5.23	162	264	4.96
164	262	4.10	163	262	4.58	163	263	4.54	163	264	4.97	163	265	4.71
165	263	3.97	164	263	4.20	164	264	4.14	164	265	4.56	164	266	4.29
166	264	3.71	165	264	3.99	165	265	3.85	165	266	4.15	165	267	3.86
167	265	3.71	166	265	3.78	166	266	3.62	166	267	3.92	166	268	3.69
168	266	3.62	167	266	3.65	167	267	3.51	167	268	3.64	167	269	3.52
169	267	4.38	168	267	3.50	168	268	3.38	168	269	3.55	168	270	3.27
170	268	3.85	169	268	3.78	169	269	3.84	169	270	3.69	169	271	3.51
171	269	4.81	170	269	3.52	170	270	3.43	170	271	3.35	170	272	3.19
172	270	4.48	171	270	4.20	171	271	4.36	171	272	3.92	171	273	3.93
173	271	5.13	172	271	3.79	172	272	3.94	172	273	3.50	172	274	3.46
174	272	5.13	173	272	4.46	173	273	4.62	173	274	4.31	173	275	4.08
175	273	6.00	174	273	4.31	174	274	4.48	174	275	3.99	174	276	3.91
176	274	5.58	175	274	5.18	175	275	5.37	175	276	4.87	175	277	4.72
177	275	6.63	176	275	4.89	176	276	5.01	176	277	4.60	176	278	4.39
178	276	6.17	177	276	6.10	177	277	6.01	177	278	5.56	177	279	5.41
179	277	6.72	178	277	5.41	178	278	5.52	178	279	5.04	178	280	4.86
180	278	6.49	179	278	6.03	179	279	5.99	179	280	5.43	179	281	5.37
181	279	7.85	180	279	5.73	180	280	5.66	180	281	5.10	180	282	5.04
182	280	6.93	181	280	6.50	181	281	6.41	181	282	5.71	181	283	6.22
183	281	7.65	182	281	5.99	182	282	5.96	182	283	5.13	182	284	5.31
184	282	7.14	183	282	6.68	183	283	6.65	183	284	5.95	183	285	6.11
185	283	5.73	184	283	6.19	184	284	6.17	184	285	5.36	184	286	5.48
186	284	5.43	185	284	4.79	185	285	4.70	185	286	4.29	185	287	4.29
187	285	4.59	186	285	4.54	186	286	4.47	186	287	4.02	186	288	3.97
188	286	4.00	187	286	3.76	187	287	3.60	187	288	3.38	187	289	3.20
189	287	4.13	188	287	3.30	188	288	3.09	188	289	3.00	188	290	2.73
190	288	3.52	189	288	3.30	189	289	3.10	189	290	2.88	189	291	2.48
191	289	3.53	190	289	2.79	190	290	2.48	190	291	2.42	190	292	2.09
192	290	3.08	191	290	2.69	191	291	2.57	191	292	2.64	191	293	2.24
			192	291	2.17	192	292	2.05	192	293	2.13	192	294	1.73

TABLE IV: Calculated fission barrier heights (in MeV).

N	A	$B_f$	N	A	$B_f$	N	A	$B_f$	N	A	$B_f$	N	A	$B_f$
<b>Z=103</b>			<b>Z=104</b>			<b>Z=105</b>			<b>Z=106</b>			<b>Z=107</b>		
139	242	3.13												
140	243	3.14	140	244	2.69									
141	244	4.01	141	245	3.58	141	246	2.89						
142	245	3.92	142	246	3.46	142	247	3.09	142	248	2.66			
143	246	4.55	143	247	4.16	143	248	3.77	143	249	3.37	143	250	3.30
144	247	4.66	144	248	4.13	144	249	3.75	144	250	3.35	144	251	3.31
145	248	5.29	145	249	4.95	145	250	4.68	145	251	4.21	145	252	4.17
146	249	5.19	146	250	4.74	146	251	4.56	146	252	4.15	146	253	4.16
147	250	6.10	147	251	5.47	147	252	5.57	147	253	5.01	147	254	5.19
148	251	5.79	148	252	5.36	148	253	5.62	148	254	4.98	148	255	5.08
149	252	6.54	149	253	6.16	149	254	6.77	149	255	5.98	149	256	6.22
150	253	6.28	150	254	5.93	150	255	6.43	150	256	5.76	150	257	5.92
151	254	7.26	151	255	6.93	151	256	7.50	151	257	6.85	151	258	7.17
152	255	6.81	152	256	6.44	152	257	7.04	152	258	6.37	152	259	6.70
153	256	6.62	153	257	6.36	153	258	7.18	153	259	6.58	153	260	6.83
154	257	6.45	154	258	6.11	154	259	6.99	154	260	6.49	154	261	6.70
155	258	6.49	155	259	6.14	155	260	7.18	155	261	6.61	155	262	6.69
156	259	6.30	156	260	5.96	156	261	6.82	156	262	6.30	156	263	6.53
157	260	6.33	157	261	6.01	157	262	6.84	157	263	6.37	157	264	6.74
158	261	6.10	158	262	5.73	158	263	6.56	158	264	6.03	158	265	6.44
159	262	6.15	159	263	5.68	159	264	6.53	159	265	5.97	159	266	6.92
160	263	5.89	160	264	5.45	160	265	6.31	160	266	5.83	160	267	6.72
161	264	6.36	161	265	5.91	161	266	6.83	161	267	6.45	161	268	7.60
162	265	5.83	162	266	5.46	162	267	6.40	162	268	5.95	162	269	7.20
163	266	5.19	163	267	5.14	163	268	5.99	163	269	5.69	163	270	6.95
164	267	4.83	164	268	4.59	164	269	5.37	164	270	5.06	164	271	6.27
165	268	4.17	165	269	4.13	165	270	4.71	165	271	4.50	165	272	5.61
166	269	3.97	166	270	3.85	166	271	4.43	166	272	4.17	166	273	5.30
167	270	3.82	167	271	3.67	167	272	4.00	167	273	3.85	167	274	4.67
168	271	3.41	168	272	3.33	168	273	3.70	168	274	3.54	168	275	4.38
169	272	3.52	169	273	3.44	169	274	3.67	169	275	3.44	169	276	3.93
170	273	3.19	170	274	3.12	170	275	3.37	170	276	3.20	170	277	3.72
171	274	3.68	171	275	3.65	171	276	3.81	171	277	3.56	171	278	4.11
172	275	3.30	172	276	3.20	172	277	3.36	172	278	3.24	172	279	3.70
173	276	4.07	173	277	3.83	173	278	4.08	173	279	3.89	173	280	4.33
174	277	3.67	174	278	3.48	174	279	3.72	174	280	3.55	174	281	4.10
175	278	4.55	175	279	4.55	175	280	4.73	175	281	4.71	175	282	5.15
176	279	4.00	176	280	4.12	176	281	4.10	176	282	4.15	176	283	4.64
177	280	4.97	177	281	5.24	177	282	5.03	177	283	5.29	177	284	5.27
178	281	4.46	178	282	4.77	178	283	4.51	178	284	4.78	178	285	4.65
179	282	5.01	179	283	5.19	179	284	5.23	179	285	5.26	179	286	5.49
180	283	4.68	180	284	4.89	180	285	4.75	180	286	5.06	180	287	4.99
181	284	5.62	181	285	5.69	181	286	5.71	181	287	5.83	181	288	5.84
182	285	5.00	182	286	5.17	182	287	5.13	182	288	5.22	182	289	5.27
183	286	5.91	183	287	5.89	183	288	5.87	183	289	6.01	183	290	6.13
184	287	5.31	184	288	5.36	184	289	5.34	184	290	5.41	184	291	5.52
185	288	4.38	185	289	4.27	185	290	4.32	185	291	4.26	185	292	4.25
186	289	4.17	186	290	4.01	186	291	4.11	186	292	4.11	186	293	4.26
187	290	2.74	187	291	3.05	187	292	3.24	187	293	2.99	187	294	3.19
188	291	2.76	188	292	2.57	188	293	2.83	188	294	2.67	188	295	2.91
189	292	2.44	189	293	2.23	189	294	2.18	189	295	1.88	189	296	1.86
190	293	2.20	190	294	1.81	190	295	1.92	190	296	1.56	190	297	1.61
191	294	2.21	191	295	1.89	191	296	1.73	191	297	1.48	191	298	1.40
192	295	1.70	192	296	1.44	192	297	1.37	192	298	1.12	192	299	1.06

TABLE V: Calculated fission barrier heights (in MeV).

N	A	$B_f$	N	A	$B_f$	N	A	$B_f$	N	A	$B_f$	N	A	$B_f$
Z=108			Z=109			Z=110			Z=111			Z=112		
144	252	2.72												
145	253	3.49	145	254	2.72									
146	254	3.58	146	255	3.06	146	256	2.47						
147	255	4.50	147	256	3.71	147	257	3.29	147	258	2.60			
148	256	4.48	148	257	3.70	148	258	3.32	148	259	2.50	148	260	2.21
149	257	5.60	149	258	4.88	149	259	4.26	149	260	3.33	149	261	2.96
150	258	5.29	150	259	4.53	150	260	4.05	150	261	3.27	150	262	2.77
151	259	6.40	151	260	5.53	151	261	5.12	151	262	4.10	151	263	3.92
152	260	5.98	152	261	5.17	152	262	4.68	152	263	3.67	152	264	3.47
153	261	6.13	153	262	5.00	153	263	4.68	153	264	3.73	153	265	3.40
154	262	6.07	154	263	4.97	154	264	4.50	154	265	3.81	154	266	3.34
155	263	6.07	155	264	5.01	155	265	4.50	155	266	3.65	155	267	3.22
156	264	5.93	156	265	4.92	156	266	4.39	156	267	3.74	156	268	3.26
157	265	6.09	157	266	5.29	157	267	4.50	157	268	3.65	157	269	3.21
158	266	5.83	158	267	5.11	158	268	4.38	158	269	3.68	158	270	3.31
159	267	6.19	159	268	5.85	159	269	5.04	159	270	4.52	159	271	3.98
160	268	5.93	160	269	5.65	160	270	4.86	160	271	4.26	160	272	3.78
161	269	6.87	161	270	6.72	161	271	5.91	161	272	5.58	161	273	5.02
162	270	6.46	162	271	6.44	162	272	5.62	162	273	5.30	162	274	4.72
163	271	6.28	163	272	6.48	163	273	5.85	163	274	5.70	163	275	5.00
164	272	5.52	164	273	5.85	164	274	5.22	164	275	5.03	164	276	4.46
165	273	5.00	165	274	5.56	165	275	4.87	165	276	5.05	165	277	4.46
166	274	4.62	166	275	5.14	166	276	4.47	166	277	4.62	166	278	4.01
167	275	4.16	167	276	4.90	167	277	4.16	167	278	4.61	167	279	3.99
168	276	3.80	168	277	4.45	168	278	3.73	168	279	4.13	168	280	3.78
169	277	3.40	169	278	4.14	169	279	3.44	169	280	4.35	169	281	3.88
170	278	3.20	170	279	3.84	170	280	3.29	170	281	4.19	170	282	3.74
171	279	3.80	171	280	4.09	171	281	3.95	171	282	4.74	171	283	4.58
172	280	3.31	172	281	3.87	172	282	3.72	172	283	4.67	172	284	4.34
173	281	4.20	173	282	4.55	173	283	4.68	173	284	5.32	173	285	5.26
174	282	3.88	174	283	4.22	174	284	4.40	174	285	5.07	174	286	5.03
175	283	5.00	175	284	5.37	175	285	5.51	175	286	5.83	175	287	6.04
176	284	4.50	176	285	4.91	176	286	5.04	176	287	5.37	176	288	5.60
177	285	5.43	177	286	5.74	177	287	5.86	177	288	6.39	177	289	6.29
178	286	4.93	178	287	5.17	178	288	5.33	178	289	5.93	178	290	5.87
179	287	5.61	179	288	6.03	179	289	5.96	179	290	6.60	179	291	6.32
180	288	5.29	180	289	5.66	180	290	5.61	180	291	6.23	180	292	5.94
181	289	6.06	181	290	6.19	181	291	6.12	181	292	6.59	181	293	6.29
182	290	5.47	182	291	5.70	182	292	5.63	182	293	6.18	182	294	5.89
183	291	6.05	183	292	6.46	183	293	6.20	183	294	6.75	183	295	6.48
184	292	5.61	184	293	5.95	184	294	5.68	184	295	6.20	184	296	5.91
185	293	4.20	185	294	4.51	185	295	4.38	185	296	4.79	185	297	4.54
186	294	4.23	186	295	4.68	186	296	4.50	186	297	5.04	186	298	4.74
187	295	3.04	187	296	3.09	187	297	3.07	187	298	3.73	187	299	3.39
188	296	2.83	188	297	3.11	188	298	3.01	188	299	3.76	188	300	3.44
189	297	1.75	189	298	1.80	189	299	1.79	189	300	2.20	189	301	1.92
190	298	1.44	190	299	1.74	190	300	1.58	190	301	2.28	190	302	2.02
191	299	1.30	191	300	1.21	191	301	1.28	191	302	1.05	191	303	1.07
192	300	0.75	192	301	0.74	192	302	0.76	192	303	0.99	192	304	0.76

TABLE VI: Calculated fission barrier heights (in MeV).

N	A	$B_f$	N	A	$B_f$	N	A	$B_f$	N	A	$B_f$	N	A	$B_f$
<b>Z=113</b>			<b>Z=114</b>			<b>Z=115</b>			<b>Z=116</b>			<b>Z=117</b>		
149	262	2.02												
150	263	2.02	150	264	1.72									
151	264	2.95	151	265	2.75	151	266	1.54						
152	265	2.44	152	266	2.27	152	267	1.17	152	268	1.08			
153	266	2.33	153	267	2.15	153	268	0.90	153	269	0.96	153	270	0.76
154	267	2.25	154	268	2.14	154	269	1.34	154	270	1.01	154	271	0.87
155	268	2.44	155	269	2.13	155	270	2.14	155	271	1.39	155	272	1.93
156	269	2.34	156	270	2.27	156	271	2.29	156	272	1.72	156	273	1.99
157	270	2.55	157	271	2.36	157	272	2.81	157	273	2.24	157	274	2.58
158	271	2.66	158	272	2.50	158	273	2.89	158	274	2.37	158	275	2.91
159	272	3.65	159	273	3.25	159	274	3.67	159	275	3.13	159	276	3.33
160	273	3.45	160	274	3.39	160	275	3.81	160	276	3.27	160	277	3.69
161	274	4.58	161	275	4.53	161	276	4.88	161	277	4.45	161	278	4.74
162	275	4.41	162	276	4.35	162	277	4.68	162	278	4.18	162	279	4.35
163	276	4.88	163	277	4.75	163	278	5.30	163	279	4.77	163	280	5.10
164	277	4.44	164	278	4.32	164	279	4.79	164	280	4.34	164	281	4.66
165	278	4.58	165	279	4.29	165	280	4.87	165	281	4.36	165	282	4.47
166	279	4.23	166	280	3.99	166	281	4.56	166	282	4.16	166	283	4.53
167	280	4.67	167	281	4.37	167	282	4.96	167	283	4.52	167	284	4.77
168	281	4.34	168	282	4.05	168	283	4.81	168	284	4.48	168	285	4.69
169	282	4.89	169	283	4.52	169	284	5.29	169	285	4.83	169	286	5.23
170	283	4.46	170	284	4.48	170	285	4.98	170	286	4.70	170	287	5.30
171	284	5.19	171	285	5.16	171	286	5.70	171	287	5.76	171	288	6.21
172	285	4.98	172	286	4.83	172	287	5.56	172	288	5.45	172	289	5.95
173	286	5.74	173	287	5.76	173	288	6.21	173	289	6.18	173	290	6.81
174	287	5.54	174	288	5.52	174	289	6.02	174	290	5.93	174	291	6.46
175	288	6.43	175	289	6.43	175	290	6.68	175	291	6.67	175	292	7.04
176	289	6.28	176	290	6.04	176	291	6.55	176	292	6.31	176	293	6.56
177	290	6.95	177	291	6.67	177	292	7.46	177	293	6.82	177	294	7.31
178	291	6.61	178	292	6.58	178	293	6.80	178	294	6.37	178	295	6.64
179	292	7.26	179	293	6.75	179	294	7.08	179	295	6.64	179	296	6.88
180	293	6.82	180	294	6.45	180	295	6.69	180	296	6.25	180	297	6.32
181	294	6.93	181	295	6.64	181	296	7.00	181	297	6.51	181	298	6.70
182	295	6.71	182	296	6.29	182	297	6.48	182	298	6.10	182	299	6.12
183	296	7.13	183	297	6.58	183	298	6.75	183	299	6.35	183	300	6.32
184	297	6.63	184	298	6.10	184	299	6.23	184	300	5.84	184	301	5.81
185	298	5.36	185	299	4.72	185	300	4.97	185	301	4.39	185	302	4.27
186	299	5.43	186	300	4.92	186	301	5.01	186	302	4.64	186	303	4.61
187	300	4.11	187	301	3.52	187	302	3.85	187	303	3.27	187	304	3.32
188	301	4.14	188	302	3.66	188	303	3.74	188	304	3.40	188	305	3.34
189	302	2.67	189	303	2.26	189	304	2.53	189	305	2.04	189	306	2.28
190	303	2.70	190	304	2.36	190	305	2.34	190	306	2.16	190	307	2.07
191	304	1.30	191	305	0.78	191	306	1.53	191	307	0.90	191	308	1.25
192	305	1.28	192	306	0.91	192	307	1.23	192	308	0.75	192	309	1.18



TABLE VII: Calculated fission barrier heights (in MeV).

N	A	$B_f$	N	A	$B_f$	N	A	$B_f$	N	A	$B_f$	N	A	$B_f$
<b>Z=118</b>			<b>Z=119</b>			<b>Z=120</b>			<b>Z=121</b>			<b>Z=122</b>		
154	272	0.66												
155	273	1.39	155	274	1.82									
156	274	1.41	156	275	1.83	156	276	1.38						
157	275	2.30	157	276	2.26	157	277	1.79	157	278	1.96			
158	276	2.25	158	277	2.25	158	278	1.88	158	279	2.11	158	280	1.47
159	277	3.06	159	278	2.78	159	279	2.39	159	280	2.72	159	281	1.94
160	278	3.15	160	279	2.79	160	280	2.44	160	281	2.75	160	282	2.15
161	279	4.30	161	280	3.49	161	281	3.23	161	282	3.66	161	283	3.07
162	280	3.94	162	281	3.27	162	282	3.07	162	283	3.50	162	284	2.94
163	281	4.32	163	282	3.96	163	283	3.89	163	284	4.56	163	285	3.88
164	282	4.13	164	283	3.68	164	284	3.57	164	285	4.16	164	286	3.61
165	283	3.79	165	284	3.87	165	285	3.65	165	286	4.67	165	287	4.46
166	284	3.64	166	285	3.67	166	286	3.43	166	287	4.36	166	288	3.91
167	285	4.09	167	286	4.43	167	287	4.08	167	288	4.40	167	289	4.06
168	286	4.01	168	287	4.45	168	288	4.21	168	289	4.37	168	290	4.01
169	287	5.03	169	288	5.21	169	289	5.01	169	290	5.35	169	291	4.83
170	288	5.05	170	289	5.23	170	290	5.01	170	291	5.41	170	292	4.80
171	289	6.03	171	290	6.26	171	291	6.08	171	292	6.56	171	293	5.96
172	290	5.75	172	291	5.75	172	292	5.48	172	293	5.90	172	294	5.36
173	291	6.40	173	292	6.55	173	293	6.06	173	294	6.15	173	295	5.54
174	292	6.09	174	293	6.21	174	294	5.62	174	295	5.89	174	296	5.28
175	293	6.62	175	294	6.95	175	295	6.28	175	296	6.00	175	297	5.48
176	294	6.09	176	295	6.32	176	296	5.79	176	297	5.69	176	298	5.10
177	295	6.64	177	296	6.71	177	297	6.02	177	298	5.90	177	299	5.36
178	296	6.12	178	297	6.20	178	298	5.56	178	299	5.38	178	300	4.86
179	297	6.21	179	298	6.20	179	299	5.57	179	300	5.38	179	301	4.75
180	298	5.79	180	299	5.72	180	300	5.08	180	301	4.82	180	302	4.26
181	299	6.02	181	300	5.88	181	301	5.24	181	302	4.99	181	303	4.43
182	300	5.52	182	301	5.38	182	302	4.71	182	303	4.37	182	304	3.78
183	301	5.71	183	302	5.50	183	303	4.81	183	304	4.27	183	305	3.70
184	302	5.20	184	303	4.98	184	304	4.30	184	305	3.64	184	306	3.16
185	303	3.93	185	304	3.82	185	305	3.02	185	306	2.96	185	307	2.27
186	304	4.03	186	305	3.85	186	306	3.14	186	307	2.60	186	308	2.08
187	305	2.80	187	306	2.78	187	307	2.17	187	308	2.15	187	309	1.66
188	306	2.78	188	307	2.63	188	308	1.95	188	309	1.84	188	310	1.50
189	307	1.78	189	308	2.03	189	309	1.51	189	310	1.50	189	311	1.31
190	308	1.57	190	309	1.97	190	310	1.39	190	311	1.45	190	312	1.15
191	309	0.79	191	310	1.67	191	311	1.05	191	312	1.20	191	313	0.68
192	310	0.80	192	311	1.63	192	312	1.05	192	313	1.28	192	314	0.80

TABLE VIII: Calculated fission barrier heights (in MeV).

N	A	$B_f$	N	A	$B_f$	N	A	$B_f$	N	A	$B_f$
<b>Z=123</b>			<b>Z=124</b>			<b>Z=125</b>			<b>Z=126</b>		
159	282	2.14									
160	283	2.25	160	284	1.78						
161	284	3.01	161	285	2.51	161	286	2.47			
162	285	2.87	162	286	2.44	162	287	2.44	162	288	1.89
163	286	4.03	163	287	3.46	163	288	3.18	163	289	2.64
164	287	3.69	164	288	3.24	164	289	3.18	164	290	2.58
165	288	4.75	165	289	4.43	165	290	4.43	165	291	3.85
166	289	4.15	166	290	3.78	166	291	3.76	166	292	3.24
167	290	4.43	167	291	4.08	167	292	4.14	167	293	3.69
168	291	4.08	168	292	3.54	168	293	3.64	168	294	3.15
169	292	5.10	169	293	4.44	169	294	4.34	169	295	3.48
170	293	4.94	170	294	4.38	170	295	4.35	170	296	3.49
171	294	5.96	171	295	5.44	171	296	5.47	171	297	4.62
172	295	5.52	172	296	5.01	172	297	5.06	172	298	4.20
173	296	5.52	173	297	5.10	173	298	5.30	173	299	4.84
174	297	5.23	174	298	4.81	174	299	5.02	174	300	4.52
175	298	5.16	175	299	4.82	175	300	5.13	175	301	4.65
176	299	4.82	176	300	4.51	176	301	4.76	176	302	4.37
177	300	5.26	177	301	4.92	177	302	5.14	177	303	4.75
178	301	4.75	178	302	4.48	178	303	4.66	178	304	4.28
179	302	4.83	179	303	4.55	179	304	4.68	179	305	4.33
180	303	4.07	180	304	3.84	180	305	4.03	180	306	3.66
181	304	3.90	181	305	3.39	181	306	3.45	181	307	2.96
182	305	3.39	182	306	2.95	182	307	3.17	182	308	2.79
183	306	3.54	183	307	2.78	183	308	3.02	183	309	2.21
184	307	2.91	184	308	2.25	184	309	2.53	184	310	2.08
185	308	2.20	185	309	2.07	185	310	2.40	185	311	2.05
186	309	2.01	186	310	1.96	186	311	2.37	186	312	1.90
187	310	1.89	187	311	1.69	187	312	1.90	187	313	1.39
188	311	1.85	188	312	1.62	188	313	1.76	188	314	1.26
189	312	1.47	189	313	1.16	189	314	1.36	189	315	0.90
190	313	1.31	190	314	0.98	190	315	1.10	190	316	0.80
191	314	0.90	191	315	0.68	191	316	0.91	191	317	0.81
192	315	0.76	192	316	0.62	192	317	0.84	192	318	0.70